

This is an Open Access document downloaded from ORCA, Cardiff University's institutional repository: <https://orca.cardiff.ac.uk/id/eprint/155451/>

This is the author's version of a work that was submitted to / accepted for publication.

Citation for final published version:

Fantong, Wilson Y., Chounna, Gergino, Nenkam, Therese.L.L. Jokam, Fouepe, Alain T., Fru, Ernest Chi, Vassolo, Sara, Montcoudiol, Nelly, Fodoue, Yaya, Haman, Jean Blaise D., Carlier, Claire, Nbandah, Pierre and Nkeng, George E. 2023. Hydrogeochemistry of low agricultural soil yield in Sahelian and sub-tropical watersheds, Northern Cameroon. Journal of African Earth Sciences 199 , 104823.  
10.1016/j.jafrearsci.2022.104823

Publishers page: <http://dx.doi.org/10.1016/j.jafrearsci.2022.104823>

Please note:

Changes made as a result of publishing processes such as copy-editing, formatting and page numbers may not be reflected in this version. For the definitive version of this publication, please refer to the published source. You are advised to consult the publisher's version if you wish to cite this paper.

This version is being made available in accordance with publisher policies. See <http://orca.cf.ac.uk/policies.html> for usage policies. Copyright and moral rights for publications made available in ORCA are retained by the copyright holders.



# Hydrogeochemistry of low agricultural soil yield in Sahelian and sub-tropical watersheds, Northern Cameroon

Wilson Y. FANTONG<sup>1</sup><sup>Ω</sup>, Gergino CHOUNNA<sup>2</sup>, Therese L. L. Jokam NENKAM<sup>3</sup>, Alain T. FOUEPE<sup>1</sup>, Ernest CHI FRU<sup>4</sup>, Sara VASSOLO<sup>5</sup>, Nelly MONTCOUDIOL<sup>5</sup>, Yaya FODOUE<sup>1</sup>, Jean Blaise D. HAMAN<sup>6</sup>, Claire CARLIER<sup>3,5</sup>, Pierre NBENDAH<sup>7</sup>, George E. NKENG<sup>2</sup>

<sup>1</sup> Institute for Geological and Mining Research, Box 4110, Yaoundé, Cameroon

<sup>2</sup> Department of Environmental Engineering, National Advanced School of Public Works, Yaoundé. Box 510 Yaoundé, Cameroon

<sup>3</sup>Federal Institute of Geoscience and Natural Resources (BGR). P.O. Box 169, Yaoundé, Cameroon

<sup>4</sup> School of Earth and Environmental Sciences, Centre for Geobiology and Geochemistry, Cardiff University, Cardiff, Park Place, CF 10 3AT, Wales, UK

<sup>5</sup> Federal Institute of Geoscience and Natural Resources (BGR), GeoZentrum - Hannover, Stilleweg 2, 30655, Hannover-Germany

<sup>6</sup> University of Maroua, Box 46 Maroua, Cameroon

<sup>7</sup> University of Yaoundé I. Box 812, Yaoundé, Cameroon

<sup>Ω</sup> Corresponding author: [fantongy@gmail.com](mailto:fantongy@gmail.com)

## ABSTRACT

Bound to the north by the Sahara and to the south by the Sudanian savannah, watersheds in the African Sahelian belt supply food and water to an estimated 135 million people. Being one of the Earth's most vulnerable zones to climate change impacts, the Sahel covers a 3.1 million km<sup>2</sup> corridor from the Atlantic Ocean in the west to the Red Sea in the east. It is predicted that decadal timescale migration of Sahelian arid conditions southwards, and associated changes in water-rock interaction patterns resulting from desertification and reduction in rainfall trends, would increasingly alter soil nutrients availability. In this pilot study, we developed a hydrogeochemical approach by linking local geology to elemental dynamics, while focusing on nutrient enrichment, depletion, mobility, flux, and exchange between bedrock and groundwater. This approach was successfully applied to two watersheds in Northern Cameroon: the Sahelian Douka Longo sedimentary watershed (SDLSW) and the tropical Bidou igneous watershed (TBIW). Comparative inorganic nutrient budgets and availability suggest that carbonates and plagioclases are prone to weak and intermediate chemical weathering, compared to stronger rates recorded for granite, basalt, trachyte, and sandstone. Collectively, these sources contribute to significant trace element nutrients enrichment of local water bodies within the watersheds. Non-isochemical dissolution produces highly mobile Ca, Mn, Na, Cu, Zn, K, Ni and Fe compared to elements not part of plant nutrients. Acidic groundwater recharged by rainwater through preferential flow pass has a Ca+Mg-NO<sub>3</sub> and Ca+Mg-HCO<sub>3</sub> chemical signature in the SDLSW and the TBIW, respectively. Both watersheds are characterised by distinct solute flux patterns, with lower annual nutrient loss rates associated with the TBIW. The data indicate that surface water runoff needs to be managed to control nutrient deficiencies and excesses, and that low-yield capacity in both watersheds appear to be partly linked to P, Fe, and Mo deficiencies.

**Key words:** *Northern Cameroon. Chemical weathering. Chemical flux. Inorganic soil nutrients.*

## 1. INTRODUCTION

The ca. 3.1 million km<sup>2</sup> Sahelian belt (Fig.1) represents a unique climatic system marked by a transition from semi-arid (Sahara Desert to the north) to sub-humid (Sudanian savannah to the south) conditions. Within this corridor, tributaries of the Lake Chad and Niger River dendritically drain the main agro-ecological zone of the Far North and North Regions of Cameroon, Central Africa. These regions are vulnerable to the impact of climate change and the variability associated with rising atmospheric temperatures, decreasing rainfall, desertification, and flash floods (Chabejong, 2016; Dassou et al., 2016; Epule et al., 2018).

Integrated ecosystem management approaches on watershed have been proposed to evaluate the environmental impacts of human activities for temperate zones (Drever and Clow, 1995; Moldan and Cerny, 1994), but very rarely for the tropics (Bruijnzeel, 1990; Thomas, 1994; White and Blum, 1995), and Sahelian zones (Fantong et al., 2020). This management approach has been successfully applied to small hydrologic and topographically well-defined watersheds covering tens to thousands of hectares (e.g., Paces, 1983; Siegel and Pfannkuch, 1984; White et al., 1999).

This study carried out a pilot test in the Douka Longo Sahelian and Bidou tropical-Sahelian transitional watershed regions of Northern Cameroon (Fig. 1). The Sahelian Douka Longo sedimentary watershed (SDLSW, North Region) and the tropical Bidou igneous watershed (TBIW; Adamawa Region) (Fig. 1) produce maize, yams, potatoes, peanuts, and sorghum that represent an important stable food and income sources for the local population. Similar activities are common across the entire Sahel region, which is characterised by homogeneous climate, topography, geomorphology and soils. As a basis for this study, it is assumed that persistent poor agricultural outputs in the SDLSW and TBIW, reported by farmers and agriculture stakeholders to Cameroon's Institute for Agricultural and Rural Development (IRAD, 2018) is due to soil nutrients deficiency (Forth, 1984).

Carbonic acid resulting from the dissolution of atmospheric carbon dioxide in rainwater and from biological respiration of organic carbon, into water bodies, makes water a potent geological solvent (Nisha et al., 2021). As a result, congruent and/or incongruent dissolution of primary and secondary rock minerals occurs and has been identified as an important geochemical mechanism by which elements are released to soil horizons through water-rock interaction (Forth, 1984). Such dissolution reactions release, transport, and distribute nutrients as a function of geochemical gradients prevailing within a watershed (Faure, 1991).

Consequently, hydrogeochemical research on water-rock interaction and elemental enrichment in soils with or without agricultural activity (Hausrath et al., 2009), has led to significant body of literature on this subject. Among others, can be cited, the behaviour of elements in weathering profiles developed from Quaternary volcanic rocks (Cotten et al., 1995; Hill et al., 2000; Little and Aeolus Lee; 2006; Nesbitt and Wilson, 1992; Patino et al., 2003; Price et al., 1991; Quantin et al., 1991); the behaviour of elements in soils developed from nephelinitic rocks at Mt. Etinde in Cameroon (Etame et al., 2009); solute generation during silicate weathering in Japan (Vuai and Tokuyama, 2007); mobility and fluxes of elements during basalt weathering at Mt. Etna, Italy (Aiuppa et al., 2000); trace metal modelling of groundwater-gas-rock interaction in a volcanic aquifer (Aiuppa et al., 2005); weathering rates of granitoids in humid tropical watersheds (Braun et al., 2005); chemical alteration and resulting clay minerals formed when fresh rocks are weathered (Andrews et al., 2004); implications of water-rock interaction on the failure of the Lake Nyos natural dam (Fantong et al., 2015); compositions and mobility of elements in the Benue River Basin in Cameroon (Fantong et al., 2020); quantification of elemental fluxes behaviour of chemical element fractionation during silicate rock weathering processes (White and Brantley, 1995); enrichment and depletion of elements in altered rocks within hydrochemical systems (Brimhall and Dietrich, 1987); rare earth elements variation in agricultural fields from eroded granitic hilly lands in southern China (Chen et al., 2019); bioaccumulation and translocation of rare earth elements (REEs) in two forage legumes grown in soils treated with coal fly ash (He et al., 2019); geochemistry and recharge mechanisms of groundwater from the Garoua sandstone aquifer in north Cameroon (Njitchoua et al., 1997); and integrated and sustainable management of shared aquifer systems and basins of the Sahel region (Huneau et al., 2017). These references discuss chemical weathering of bedrock minerals contribution to the abundance and availability of nutrients in soil horizons, which in turn determines crop yields (Dehnavi et al., 2011). However, there is a paucity of comprehensive hydrogeochemical investigation linking elements derived from water-rock interactions to nutrient availability behaviour in watersheds for most of the 3.1 million km<sup>2</sup> Sahelian zone (Jokam Nenkam et al., 2022). Such studies are required to evaluate how changing rainfall patterns affect the distribution of soil nutrients, and to provide crucial information for the mitigation of climate-related impacts on agricultural productivity, thus enabling the development of sustainable livelihoods practices.

Against this backdrop, the present study compares elemental geochemistry of major ions, silica composition, stable isotopes, trace elements, and REEs in surface and groundwater and rocks

to assess the mobility, enrichment, and depletion of elements in the two agricultural watersheds previously cited (SDLSW, North Region and TBIW, Adamawa Region, both in Cameroon). The study aims to identify (1) chemical weathering types and rates, (2) elemental enrichment, depletion, and relative mobility from bedrock, and (3) to assess elemental contents of various catchment water bodies, and fluxes within the watersheds. The data are integrated together to predict and compare the hydrogeochemical behaviour of nutrient-generating and nutrient-limiting processes.

## **2. DESCRIPTION OF THE TWO WATERSHEDS**

### **2.1. The Sahel Douka Longo Sedimentary Watershed (SDLSW)**

The 678-km<sup>2</sup> SDLSW, in the North Region of Cameroon (Fig. 1c), sustains an agrarian population of about 2.2 million inhabitants. Situated between latitudes 8.8 and 9.1N and longitudes 13.3 and 13.5E, the SDLSW is characterized by a Sudano-Sahelian semi-arid climate (Fig. 1b), with a mean annual temperature of 28°C, reaching a maximum of 45°C in March before dropping to 19°C in December (Molua, 2006). The rain season from May to September is followed by seven months of dry season from October to April. At the peak of the dry season, the Mayo Douka and Mayo Mbangai, tributaries of the Douka Longo River, dry out, with interflow maintained at depths of about 0.5 m in the river channels, as revealed by this study. During the dry season, Harmattan winds from the Sahara deplete the sandy soil of fine-grained nutrients that are essential for agriculture. At the peak of the rainy season (August-September), the low-lying areas of the watershed, located between 197 and 285 metres above sea level (m asl), are flooded. As a result, soil inter-grain spaces are clogged with clay-sized sediments, rendering the top soil unsuitable for agricultural production and drastically limiting food supply to the 2.2 million people inhabiting the North Region (of Cameroon) and beyond.

An estimated 80% of the SDLSW drains Cretaceous siliceous, arkosic sandstones and poorly-sorted, immature, polymictic intra-formational conglomerates, rich in megascopic quartz and feldspar minerals. The intercalations of sandstones and conglomerates show graded bedding, with intra- and inter-rock beds separated by thin layers of iron oxides containing decimetric “sandstone ball” structures with a conglomerate core and sandstone crust. In some locations, a mosaic of potholes represents relics of the coarser conglomerate core weathered by surface runoff (Fig. 2). NW-SE and N-S trending joints, fractures, and faults intersect the rocks, providing pathways for recharge to the aquifers exploited by the population for domestic use

(by hand-dug wells). Quaternary alluvial/fluvial gravel, sand and clay-size sediments overlay the conglomerates and sandstones. Precambrian granites, Tertiary syenitic and basaltic intrusions outcrop in the upper section of the watershed to the south, where the tributaries of the Mbangai and Douka streams originate. The Quaternary and Cretaceous sediments and sedimentary rocks occupy the middle and lower portions of the watershed. Together with various tributaries originating from the sandstone hills that flank the western part (Fig. 1c), the Mbangai and Douka streams collect into the Douka Longo River, a tributary of the Benue River, which empties further down into the Niger River. The principal soil types in the watershed are sandy arenosols consisting of patches of oxisols, aridosols, and vertisols.

## 2.2. Tropical Bidou Igneous Watershed (TBIW)

The 61-km<sup>2</sup> TBIW (Fig. 1d), located in the Adamawa Region of Cameroon between latitudes 7.40 and 7.53N and longitudes 13.52 and 13.58E, is marked by two distinct seasons. The dry season runs from November to February and the wet season from March to October, with annual mean rainfall reaching 2000 mm (Cheo et al., 2013). Predominantly vegetated by savannah flora, the TBIW is drained dendritically by the Dang, the Madjinge, the Maso, and the Bidou streams. The Dang stream, together with discharged groundwater, form the main sources of water supply to Lake Dang, which outlet is located downstream to the confluence of the Madjinge, Maso, and Bidou streams. From here, the Bidou River starts and empties into the Bini River.

The streams carve valleys into the gentle slopes of Tertiary basaltic domes, which reach a maximal elevation of 1377 m asl in the upper part of the basin. The basaltic flow terminates abruptly to the south in a cliff-like feature at 1149 m asl, before continuing monotonously at altitudes ranging from 1149 to 1070 m asl in the middle part of the basin. The hillside is covered by regolith composed of a thick saprolite and complex polygenetic lateritic soil consisting of a mottled clay horizon, a carapace, a nodular ferruginous horizon, and a soft clayey topsoil. The thickness and distribution of these various soil layers depend on the topography. At the weathering front, the saprolitization process transforms the parent rocks into a loose variegated material. In the upper part of the saprolite, the ferruginization process leads to iron segregation, mottling, nodules, and red soil formation. Local glaebulization hardens the saprolitic remnants to form the carapace horizons. Runoff on the blanketing ferruginous lateritic carapace or “hard pan” washes off and mixes the overlying thin soil layer with organic matter, which is then deposited as Quaternary alluvium in the valleys. Precambrian potassic-rich granite outcrops

locally in the lower part of the basin. Younger basaltic flows and trachytic domes with piedmont deposits resulting from weathering intrude the older formations. Physical and chemical observations during fieldwork suggest that Al and Fe oxides that form the hardpans and lateritic oxisols are the dominant soil types. Just before the confluence of the Bidou and the Dori rivers with the Bini River (Fig. 1d), there are many fields cultivated by farmers who have experienced years of poor agricultural outputs, which has led to this area being labelled as “poor soil sites”. Thus, they are constrained to concentrate their agricultural activities within the low-lying alluvium in order to improve crop outputs.

### **3. MATERIALS AND METHODS**

#### **3.1. Site selection**

Preliminary visits to farming sites consistently reported to experience low yields, confirmed the predominance of lateritic, sandy, and clay clogged soils. Based on these pre-surveys, three main “poor soil sites” in each watershed were selected for this study (Fig. 1c-d). Multidisciplinary fieldwork combining pedologic observations, stream discharge measurements, as well as rock and water sampling for nutrients and geochemical analyses was carried out at these sites.

#### **3.2. Water and rock sampling**

Samples at both watersheds were collected in November 2019 during the rainy season. Water samples come from a variety of sources: hand-dug wells, springs, rivers, boreholes and lakes. Twenty-eight (28) samples were collected from open wells: 15 in the TBIW (depth to water varying between 3.5 and 13.7 m), and 14 in the SDLSW (depth to water between 1.3 and 12.5 m). Boreholes are relatively rare in the two watersheds and only one was sampled in each watershed. Groundwater originated from springs was also sampled (3 in the SDWL and 2 in the TIBW). Sixteen samples of surface water were collected: one from a lake in the TBIW, 15 from rivers (7 in the SDLSW and 8 in the TBIW). The coordinates (latitudes and longitudes) of the sampling locations were recorded using a 3-m accuracy Garmin 64 Global Positioning System (GPS).

Daily used hand-dug wells were sampled using a bucket attached to a rope without prior purging. Hand pumped wells and boreholes not in regular use were pumped until electrical conductivity (EC) values stabilized prior to sample collection. EC, pH, redox potential, and water temperature were measured before sample collection using a multi-meter model WTW 3320. Atmospheric temperature was measured with a custom CT-450WR thermometer. For the



hand-dug wells, the sampled water was transferred from the bucket into a jar thoroughly rinsed with large volumes of sampled water prior to collection to ease the filling of the sampling bottles. For boreholes, rivers, and springs, water samples were collected directly into sampling bottles.

After rinsing with sampling water, four 100-ml Nalgene polypropylene bottles were filled to the brim. The first bottle was filled with water filtered through a cellulose acetate 0.45- $\mu$ m membrane and preserved unacidified for the determination of anions. The second bottle was filled with filtered water and acidified to pH 2 with supra-pure HNO<sub>3</sub> for the measurement of cationic and trace elements. The third bottle for  $\delta^{18}\text{O}$  and  $\delta^2\text{H}$  analyses was filled with unfiltered water and tightly capped to avoid evaporation. The fourth bottle, also with unfiltered water, was used for alkalinity titration (acid neutralizing capacity (ANC)). ANC was determined within 10 hours of sample collection by direct acid titration with 0.02 N HCl and end-point determination using the Gran method. Samples for anions, cations and trace elements, and stable environmental isotope determination were labelled and preserved in ice-chilled boxes prior to laboratory analyses.

Land use pattern, human activities, and rock type were logged for each sampling site using a mobile Open Data Kit (ODK) smartphone application.

Seven representative rock samples for fresh granite, altered granite, fresh basalt, altered basalt, fresh trachyte, altered trachyte, and laterite were collected from the TBIW and two for sandstone and clay from the SDLSW for geochemistry and petrographic analyses.

The collected water and rock samples were dispatched to the Federal Institute for Geosciences and Natural Resources (BGR) in Hanover, Germany, for laboratory analyses.

### **3.3. Water analyses**

Major and minor elements were quantified using a Spectro Ciros inductively coupled plasma optical emission spectroscopy (ICP-OES) for cations (Ca, Mg, Na, K, Si, Fe(II)  $\pm$  1–2%), a UNICAM UV 300 photometer (NH<sub>4</sub><sup>+</sup>  $\pm$  3%) and a Dionex<sup>TM</sup> ion chromatography system ICS 3000 for anions (SO<sub>4</sub><sup>2-</sup>, Cl<sup>-</sup>, NO<sub>3</sub><sup>-</sup>, F<sup>-</sup>, Br<sup>-</sup>  $\pm$  1.5%). Commercial standard solutions are used for daily calibration and limits of quantitation are determined by 10-point calibration according to the DIN 32645 standard. Charge balances for major elements were within the limit  $\pm$  10 % for all samples.

Trace elements (TE), including REE, were measured on an Agilent 7500ce ICP-MS (mass spectrometer). Lab blanks were also analysed to monitor any analytical contamination. Details on the analytical instrumentation and methods can be found in Birke et al. (2010). For TEs, the analytical accuracy was checked from replicate measurement of several samples and by measuring the certified reference materials (CRM) standard of River Water (SLRS-4), produced by the National Research Council of Canada. The detection limits were 1 ng/L for all REEs. Analytical precision for the REEs, except for Ce and Pr, was better than 5% relative standard deviation (RSD), with a 10 and 11% RSD for Ce and Pr, respectively.

Stable environmental isotopes ratios  $\delta^2\text{H}$  and  $\delta^{18}\text{O}$  in water were determined on a PICARRO cavity ring-down laser spectrometer (CRDS model L2120-i), following the procedures described by Brand et al. (2009) and Lis et al. (2008). Samples were measured at least four times and the reported value is the mean one. The obtained stable isotope ratios are given in the conventional delta expression ( $\delta$ , ‰) relative to Vienna Standard Mean Ocean Water (VSMOW) and analytical precisions were  $\pm 1\text{‰}$  for  $\delta\text{D}$  and  $\pm 1.5\text{‰}$  for  $\delta^{18}\text{O}$ .

### **3.4. Rock analyses**

Major oxides ( $\text{SiO}_2$ ,  $\text{TiO}_2$ ,  $\text{Al}_2\text{O}_3$ ,  $\text{Fe}_2\text{O}_3$ ,  $\text{MnO}$ ,  $\text{MgO}$ ,  $\text{CaO}$ ,  $\text{Na}_2\text{O}$ ,  $\text{K}_2\text{O}$ ,  $\text{P}_2\text{O}_5$  and sulphate sulphur as  $\text{SO}_3$ ) and trace elements in the rock samples were measured by X-ray fluorescence (XRF) analysis using a Wavelength Dispersive X-ray Fluorescence (WDXRF) Spectrophotometer -700 HS according to DIN standard 51418. The loss on ignition (LOI) was calculated from the weight loss of the sample after 10 min at  $1030^\circ\text{C}$ . Samples are analysed in the form of fused tablets to ensure homogeneous element distribution. Major oxides concentrations are given in % weight (wt.%) and trace elements in mg/kg. The WDXRF measurement programme has been calibrated with more than 150 certified reference materials, including rocks, sediments, soils and ores. Many of the reference materials come from relevant institutions (United States Geological Survey – USGS, National Institute of Standards and Technology – NIST, Geological Survey of Japan – GSJ, Institute of Geophysical and Geochemical Exploration – IGGE, Zentrales Geologisches Institut – ZGI, Centre de Recherches Pétrographiques et Géochimiques – CRPG, Canadian Certified Reference Materials Project – CCRMP to name a few). The BGR laboratory also participated in successful inter-laboratory comparisons.

### **3.5. Stream discharge measurement**

A current meter No. 19069 and helix No. 18475 were used to measure stream discharge at the outlets of the Douka Longo and Bidou rivers for the SDLSW and TBIW, respectively. At each outlet, the discharge measurement was done at the peak of the dry and rainy season to have representative data for the 2019/2020 hydrological year.

### 3.6. Data Processing: use of software and normalization of data

All statistical analyses were performed with the R freeware version. 3.6.3; <http://www.r-project.org> (R Core Team, 2020) software. The Aquachem software (Waterloo Hydrogeologic) was used to draw Piper diagrams (Piper 1944) for identifying water type and REE patterns were drawn using Python. Maps were produced using ArcGIS version 10.2 and QGIS 2.18.X softwares. REEs were normalized by using the Post-Archean Average Australian Shale (PAAS) as a reference (Edet, 2004; McLennan, 1989), because shales are widely used in hypergene processes and environmental studies (Migaszewski et al., 2014) such as surface and shallow groundwater systems affected by weathering. Ce and Eu anomalies were quantified according to Noak et al. (2014) by using equations (1) and (2), respectively.

$$\frac{Ce}{Ce^*} = \frac{Ce_{PAAS}}{(La_{PAAS} + Pr_{PAAS})^{0.5}} \dots \dots \dots (1)$$

$$\frac{Eu}{Eu^*} = \frac{Eu_{PAAS}}{(Sm_{PAAS} + Gd_{PAAS})^{0.5}} \dots \dots \dots (2)$$

Normative minerals from water chemistry and mass balances were calculated to evaluate elemental losses and gains (mass balance) in altered rocks equivalents, by using Al<sub>2</sub>O<sub>3</sub> as the normalizing component, because of the conservation of Al during incongruent dissolution of aluminosilicate minerals (Faure, 1991).

Mass balances were calculated by assuming that Al<sub>2</sub>O<sub>3</sub> in the weathered substrate remains constant, because of its strong immobility during chemical weathering. Thus, increase in the concentration of Al<sub>2</sub>O<sub>3</sub> in the residue is expected following the decomposition of the rock during chemical weathering according to equation (3):

$$Percent\ concentration = \frac{Weight\ of\ constituent}{Weight\ of\ rock} \times 100 \dots \dots \dots (3)$$

where weight of constituent and weight of rock represent the percentage weight of Al<sub>2</sub>O<sub>3</sub> in altered rocks and amount of bulk rock remaining after alteration, respectively. The amounts of other remaining oxide constituents in the altered rocks were calculated by multiplying their percent concentrations in fresh rocks by a weight loss factor derived from the ratio of the

constant oxide ( $Al_2O_3$ ) concentrations in the fresh and altered rocks. The actual gains and losses of each component was determined following the systematic procedure explained in Faure (1991).

The strength of the water-rock interaction that led to the gains and losses of elements was evaluated by using the weathering index of Parker (PI; Parker, 1970) and the chemical index of alteration (CIA; Andrews et al., 2004; Nesbit and Young, 1989) as defined by equations (4) and (5), respectively, where the oxides contents are expressed in wt.%.

$$PI = \frac{2Na_2O}{0.35} + \frac{MgO}{0.9} + \frac{2K_2O}{0.25} + \frac{CaO}{0.7} \dots\dots\dots(4)$$

$$CIA = \left( \frac{Al_2O_3}{Al_2O_3 + CaO + Na_2O + K_2O} \right) \times 100 \dots\dots\dots(5)$$

The rate at which water-rock interactions occurs is estimated by calculating the chemical weathering rate (WRch) of the observed rocks using equation (6) (Boeglin and Probst, 1998; Vuai and Tokuyama, 2007).

$$WRch = \frac{QSiO_2}{So - Ss} \dots\dots\dots (6)$$

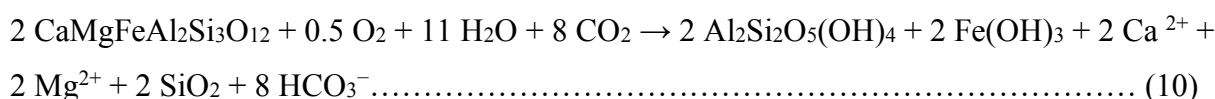
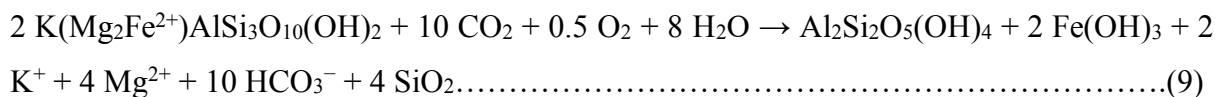
where  $QSiO_2$  is the specific flux of  $SiO_2$  ( $mol/(m^2.yr)$ ),  $So$  and  $Ss$  are the concentrations of  $SiO_2$  ( $kg/m^3$ ) in unaltered and altered rocks, respectively. A density of  $2600 kg/m^3$  was assumed for all studied rocks (granite, basalt, trachyte, and sandstone) in fresh state ( Boeglin and Probst, 1998; Dalai et al., 2002; Vuai and Tokuyama, 2007) and a density of  $1400 kg/m^3$  for those in altered state. Thus, the differences of  $SiO_2$  concentrations ( $So - Ss$ ) values are  $786 kg/m^3$ ,  $306 kg/m^3$ ,  $690 kg/m^3$ , and  $1313 kg/m^3$  for granite, basalt, trachyte and sandstone, respectively. Specific fluxes of  $SiO_2$  ( $QSiO_2$ ) are  $7.9 \times 10^{-3} mol/(m^2.yr)$  for the TBIW and  $2.1 \times 10^{-2} mol/(m^2.yr)$  for the SDLSW. The resulting weathering rates are  $6.1 \times 10^{-4} mm/yr$ ,  $1.4 \times 10^{-3} mm/yr$ ,  $6.9 \times 10^{-4} mm/yr$ , and  $5.0 \times 10^{-4} mm/yr$  for granite (TBIW), basalt (TBIW), trachyte (TBIW) and sandstone (SDLSW), respectively.

Following the procedures by Feth et al. (1964) and Garrels and Mackenzie (1967), we quantitatively determined which minerals were weathered based on the following assumptions:

1.  $H^+$  is derived by dissociation of carbonic acid in equilibrium with soil  $CO_2$  which partial pressure ( $pCO_2$ ) exceeds that of the atmosphere (Table I in Supplementary Material) due to microbial activity.

2.  $\text{Na}^+$  and  $\text{Ca}^{2+}$  cations in the connate soil water originate from the incongruent dissolution of solid-solution plagioclase (albite  $\text{NaAlSi}_3\text{O}_8$  and anorthite  $\text{CaAl}_2\text{Si}_2\text{O}_8$ ) to form kaolinite (eqn. 7 and 8 respectively).  $\text{Ca}^{2+}$  may also be derived by dissolution of secondary carbonates.
3. The weathering of biotite (eqn. 9) and ferromagnesian minerals (eqn. 10) or glass in basalt releases  $\text{Mg}^{2+}$  and  $\text{K}^+$ .  $\text{K}^+$  is also released by the weathering of K-feldspars.
4. Silicate weathering releases silicic acid.
5. Sulphate is produced by oxidation of sulphide minerals and by dissolution of gypsum/anhydrite, or originate from rainwater, alongside chloride following the dissolution of sodium chloride.
6. Bicarbonate is formed from  $\text{CO}_2$  gas and dissolution of carbonate minerals.

The dissolution reactions of key lithogenic minerals in local rocks are presented in equations 7 to 10 for albite ( $\text{NaAlSi}_3\text{O}_8$ ) anorthite ( $\text{CaAl}_2\text{Si}_2\text{O}_8$ ), biotite ( $2\text{K}(\text{Mg}_2\text{Fe}^{2+})\text{AlSi}_3\text{O}_{10}(\text{OH})_2$ ), and pyroxenes ( $\text{CaMgFeAl}_2\text{Si}_3\text{O}_{12}$ ) respectively.



The reactions of orthoclase (K-feldspars), gypsum and halite can be written in the same way. The number of moles of ions released are 1 mole of  $\text{K}^+$ , 2 moles of  $\text{SiO}_2$ , and 1 mole of  $\text{HCO}_3^-$  for orthoclase ( $\text{KAlSi}_3\text{O}_8$ ), 1 mole of  $\text{Ca}^{2+}$  and 1 mole of  $\text{SO}_4$  for gypsum ( $\text{CaSO}_4$ ), and 1 mole of  $\text{Na}^+$  and 1 mole of  $\text{Cl}^-$  for halite ( $\text{NaCl}$ ). The dissolution of halite and gypsum are considered to be congruent.

The average values for observed concentrations of ions in groundwater and surface water in the SDLSW and TBIW (Table 1), were converted from milligrams per litre to micromoles per litre. Next, the concentrations of these ions in rainwater (Table I) were subtracted. The concentrations of  $\text{SO}_4^{2-}$  and  $\text{Cl}^-$  in the analysed water sources were also taken into consideration. Before distributing the remaining ions among the minerals from which they originated, the electrical neutrality (charge) of the solutions was checked to be in excess of

+620  $\mu\text{mol}$  for the SDLSW and below neutrality by  $-31\mu\text{mol}$  for TBIW. This was then adjusted by adding or subtracting  $\text{HCO}_3^-$ .

As an example for the SDLSW, the adjusted value of  $257\mu\text{mol}$  of  $\text{Na}^+$  in one litre of water is obtained from the dissolution of  $257\mu\text{mol}$  (or  $67\text{ mg}$ ) of albite, during which  $514\mu\text{mol}$  of  $\text{SiO}_2$  and  $257\mu\text{mol}$  of  $\text{HCO}_3^-$  are consumed in accordance with eqn. (7). Next, the  $327\mu\text{mol}$  of  $\text{K}^+$  and equivalent amount of  $\text{HCO}_3^-$  were assigned to the dissolution of  $91\text{ mg}$  of K-feldspars.  $\text{SiO}_2$  could not be assigned, because it had already been consumed by albite. The  $127\mu\text{mol}$   $\text{Mg}^{2+}$  with proportional amount of  $\text{HCO}_3^-$  were assigned to the dissolution of  $28\text{ mg}$  of biotite. Consistent with the reaction of biotite described in equation (9),  $\text{SiO}_2$  and  $\text{K}^+$  were not considered because they had already been consumed by albite and K-feldspars. The  $228\mu\text{mol}$  of  $\text{Ca}^{2+}$  with proportional amount of  $\text{HCO}_3^-$  were assigned to the dissolution of  $63\text{ mg}$  of anorthite following the reaction in eqn. (8).  $\text{SO}_4^{2-}$  and  $\text{Cl}^-$ , although largely derived from atmospheric inputs and depending on a particular land use (Kringel et al., 2016), are expressed as  $0.34\text{ mg}$  of gypsum equivalents and  $14\text{ mg}$  of halite equivalents.

The percentage weight for each mineral dissolved in a litre of water was calculated for the two watersheds. The molar abundances of the considered minerals in the SDLSW are 25%, 34%, 11%, 24%, 0.13%, and 5.3% for albite, K-feldspars, biotite, anorthite, gypsum, and halite, respectively. In the TBIW, these molar abundances are 42% for albite, 29% for anorthite, 18% for biotite, 7% for K-feldspar, gypsum and halite.

The composition of dissolved plagioclase, expressed by the abundance of albite (Ab) is calculated according to equation (11) where n is the mole quantity:

$$Ab_{albite} = \frac{n_{albite}}{n_{albite} + n_{anorthite}} \times 100 \dots\dots\dots (11).$$

The abundance of albite is 53 mol% for the SDLSW and 61 mol% for the TBIW.

The extent to which major and trace elements enter the aqueous phase during chemical weathering is controlled by Bowen's reaction series (Bowen 1928). It is assessed by calculating the element relative mobility (RM) with the use of equation (12) (Gislason et al., 1996; Meybeck, 1997):

$$RM = \frac{\left(\frac{X}{Mg}\right)_w}{\left(\frac{X}{Mg}\right)_r} \dots\dots\dots (12)$$

where X/Mg is the ratio of the concentration of element X with respect to Mg concentration, w and r refer to water and rock, respectively. The water/rock concentration ratio are normalized to magnesium because of its strong chemical mobility during weathering. This approach has been successfully applied to rivers draining basaltic terrains in Iceland (e.g., Louvat, 1997), Mt. Etna in Sicily (Aiuppa et al., 2000), Mt. Vesuvius volcanic aquifer in Italy (Aiuppa et al., 2005), and sandstone terrain in Benue River Basin-Cameroon (Fantong et al., 2020). It was also applied to calculate the relative mobility of elements for 5 samples from the TBIW and 5 samples from the SDLSW. The preference to the selected samples was based on proximity to the low-yield soil sites.

Considering that the flux of elements from a watershed may contribute in determining their spatial aqueous concentration variation, which may have implications on soil nutrients availability and amelioration options, the relative flux ( $Q_i$  in mol. km<sup>-2</sup>.yr<sup>-1</sup>) of the dissolved ion i in the watershed was calculated following the procedure by Vuai and Tokuyama (2007), as shown in equation 13.

$$Q_i = \frac{C_i V_t}{A} \dots\dots\dots(13)$$

where  $C_i$  is the mean concentration (mol/L) of ion i at the outlets of rivers Bidou and Douka Longo (Fig. 1c-d);  $V_t$ , the annual average discharge (m<sup>3</sup>/s) measured at the outlets during the rain season (0.98 m<sup>3</sup>/s for SDLSW and 0.34 m<sup>3</sup>/s for TBIW); and A, the surface area (km<sup>2</sup>) of the watersheds.

## 4. RESULTS AND INTERPRETATIONS

Because of the strong relationship between agricultural output and rainfall, the study focuses on samples collected during the rainy season. Table 1 presents a statistical summary of in-situ measurements (electrical conductivity (EC), pH, water temperature) and the laboratory analytical results for major cations and anions, SiO<sub>2</sub>, stable environmental isotopes ( $\delta D$ ,  $\delta^{18}O$ ), and carbon dioxide partial pressure (pCO<sub>2</sub>) calculated using pH and HCO<sub>3</sub><sup>-</sup> (Table I). Statistical summaries of trace elements and REE in water, are presented in Tables 2 and 3, respectively. The content of major oxides and trace elements in rocks are found in Table 4.

### 4.1. Water chemistry

In the SDLSW, EC, pH, and water temperature range from 58–698  $\mu\text{S}/\text{cm}$ , 4.2–7.4, and 26.5–34.0°C, compared to TBIW values, of 9–160  $\mu\text{S}/\text{cm}$ , 5.6–7.7, and 19.5–26.1°C, respectively (Table 1 SM1a). Median water concentrations (mg/L) for major ions in the SDLSW decrease from  $\text{NO}_3^-$  (21.4) >  $\text{HCO}_3^-$  (19.9) >  $\text{Ca}^{2+}$  (8.67) >  $\text{K}^+$  (8.2) >  $\text{Na}^+$  (5.4) >  $\text{Cl}^-$  (3.71) >  $\text{Mg}^{2+}$  (2.55) >  $\text{SO}_4^{2-}$  (0.382) >  $\text{Fe}^{2+}$  (0.049) and  $\text{HCO}_3^-$  (10.0) >  $\text{Ca}^{2+}$  (1.33) >  $\text{Na}^+$  (1.1) >  $\text{K}^+$  (0.4) >  $\text{Mg}^{2+}$  (0.238) >  $\text{NO}_3^-$  (0.215) >  $\text{Cl}^-$  (0.118) >  $\text{Fe}^{2+}$  (0.054) >  $\text{SO}_4^{2-}$  (0.021) for the TBIW (Table 1). Major ions and average groundwater versus surface water concentrations (Fig. 3a and b) show that in the SDLSW groundwater is more enriched than surface water in the decreasing order  $\text{NO}_3^- > \text{K} > \text{Cl} > \text{Ca} > \text{Na} > \text{Mg} > \text{Fe} > \text{SO}_4 > \text{PO}_4$  for groundwater and  $\text{NO}_3^- > \text{Ca} > \text{K} > \text{Na} > \text{Cl} > \text{Mg} > \text{Fe} > \text{SO}_4 > \text{PO}_4$  for surface water. In TBIW, major ions are enriched in surface waters relative to groundwater with a decreasing order  $\text{Ca} > \text{Na} > \text{NO}_3^- > \text{Cl} > \text{Mg} > \text{SO}_4 > \text{K} > \text{Fe} > \text{PO}_4$  in both. These trends suggest topsoil depletion in major ions in the SDLSW occurs by water infiltration through porous sediments into the aquifer, while the TBIW loses nutrients by surface runoff to the rivers.

The concentrations of major ions correlate with calculated higher water-rock interactions in the SDLSW and are generally higher than in the TBIW. Piper diagram identifies  $\text{Ca}+\text{Mg}-\text{NO}_3$  water type as the predominant water signature in the SDLSW, and  $\text{Ca}+\text{Mg}-\text{HCO}_3$  in the TBIW (SM1b). The dominance of  $\text{NO}_3^-$  suggests strong oxidation of anthropogenic  $\text{NH}_4^+$  with potential contribution from the NPK (nitrogen, phosphorus and potassium) fertilizers commonly used in the SDLSW. The  $\text{Ca}+\text{Mg}-\text{HCO}_3$  -rich TBIW water is linked to carbonic acid dissolution of rock minerals.

The concentrations of silicic acid ( $\text{H}_4\text{SiO}_4$ ) in water samples vary from 8.7–16.2 mg/L in the SDLSW and 2.0–15.9 mg/L in the TBIW, with median values of 12.8 mg/L and 4.4 mg/L as  $\text{SiO}_2$ , respectively (Table 1). The lowest values of  $\text{H}_4\text{SiO}_4$  in the SDLSW were observed in GW001 and GW002 (Table I), which were the most acidic samples (pH of 4.2 and 4.3, respectively).

Stable isotope ratios range from –5.31 to –2.79 ‰ for  $\delta^{18}\text{O}$ , and –30.7 to –21.3 ‰ for  $\delta\text{D}$  in the SDLSW, and –4.51 to –0.86 ‰ for  $\delta^{18}\text{O}$  and –24.5 to –11.5 ‰ for  $\delta\text{D}$  in the TBIW. Research findings have reported  $\delta^{18}\text{O}$  and  $\delta\text{D}$  as conservative during water- rock interaction for low temperature water (e.g., Gat, 2010; Taylor and Howard, 1996). Thus, the  $\delta$ -values of the groundwater would be similar to that of recharging meteoric water, with soil processes climate conditions and vegetation cover as controlling factors (Adomako et al. 2015; Taylor



and Howard, 1996). Isotopes plot as a cluster along the GMWL (Global Meteoric Water Line; Craig 1961): water from the TBIW is relatively more enriched than from the SDLSW (SM2a). One sample from a spring and two from rivers in the SDLSW, as well as the sample from the lake in the TBIW plot to the right of the GMWL, indicating that surface water suffers from evaporation. The aquifer may be recharged by two possible mechanisms: preferential flow paths or homogenous diffuse recharge (Asai et al., 2010; Tsujimura et al., 2007). These mechanisms have been documented in the SDLSW (Njitchoua et al., 1995), in the Lake Chad basin (Fantong et al., 2010; Goni et al., 2006), and in coastal sedimentary basins of Cameroon (Fantong et al., 2016). Moreover, the high d-excess in surface water and groundwaters with values equal or above 10‰ in ca. 70% and >95% of water samples from the SDLSW and TBIW, respectively (SM2b), suggest that groundwater recharge occurs under high relative humidity and low temperature (Kebede et al., 2005; Kendall and Doctor, 2011).

The low pH samples GW001 (pH 4.2) and GW002 (pH 4.3) from the SDLSW and their high concentrations for most trace elements, suggest that water-rock interaction under hyper-acidic conditions promote their release from rocks. Although the median pH for both watersheds is similar (SM1a), this observation is supported by the highest trace element concentrations in the more acidic SDLSW water samples compared to the TBIW (Table 2).

The medians for the macronutrients N, K, S and P (Table 1) are in the range of <0.03–21.4 mg/L and decrease in the order  $N > K > S > P$  in the SDLSW compared to <0.03–0.4 mg/L with a  $K > N > S > P$  distribution for the TBIW.

Trace nutrients such as B, Cu, Mn, Mo, Ni, and Zn (Table 2) have a <0.020–46.1 µg/L median range that decreased in the order  $Mn > Zn > B > Ni > Cu > Mo$  in the SDLSW, against <0.020–33.7 µg/L with a similar pattern (Zn dominates instead of Mn) in the TBIW. Trace nutrients show similar patterns in both watersheds (Fig. 3c and d). However, surface water concentrations are higher in the SDLSW (Fig. 3c) and slightly lower in TBIW (Fig. 3d) than observed for groundwaters. Unlike with major ions, the top soil in the SDLSW may lose trace elements to rivers through surface run-off and by infiltration into shallow groundwater aquifers in the TBIW, suggesting trace element nutrients are transported predominantly as soluble rather than as particulate material in both watersheds.

SDLSW total REEs (Table 3) vary from 0.916–1716 µg/L with  $Ce > La > Nd > Pr > Eu > Sm$  for LREEs (light REEs) and  $Gd > Dy > Er > Yb > Tb > Ho > Tm > Lu$  for HREEs (heavy REEs). Total REEs in the TBIW range from 0.085–2.37 µg/L, with  $Ce > Nd > La > Eu > Sm$

> Pr for the LREEs and same order as the SDLSW for the HREEs. PAAS normalized REEs show conspicuous “roof shaped” patterns, due to Eu positive anomalies in the water samples from both watersheds (Fig. 4). Such patterns have been previously linked to the dissolution of plagioclase in the Benue River Basin of Northern Cameroon within which the SDLSW is situated (Fantong et al., 2020). Moreover, most of the shallow groundwater samples in SDLSW (Fig. 4 a-c) show a remarkable negative Ce anomaly, indicating the oxidation of  $Ce^{3+}$  and the precipitation of  $Ce^{4+}$  from solution as  $CeO_2$  (Elderfield and Greaves, 1982; Hoyle et al., 1984). The oxidizing conditions in the shallow groundwater is consistent with the porous and permeable sandstones in the watershed. The physical conditions for rapid oxygen transport to shallow groundwater are not favoured in the TBIW, because it is mostly covered by an impermeable lateritic duricrust. Consistently, negative Ce anomalies in this locality are absent (Fig. 4d-g). The average concentrations of LREEs and HREEs for ground and surface waters in both watersheds show similar variations (Fig. 5 a-d) but REEs concentrations are higher in the SDLSW than in the TBIW. The LREEs and HREEs show preferential fractionation in groundwater compared to surface water in SDLSW, but no preferential fractionation is observed in the TBIW. Therefore, groundwater in the SDLSW appears to be a favourable geochemical sink for REEs in comparison to surface water.

#### **4.2. Major oxides and trace element in rocks**

According to rock geochemical analytical results, outcropping altered granite, basalt, trachyte and clay show both depletion and enrichment. For instance, the altered rocks have much lower MnO, MgO, CaO, Na<sub>2</sub>O, K<sub>2</sub>O, P<sub>2</sub>O<sub>5</sub>, and Fe<sub>2</sub>O<sub>3</sub> concentrations than fresh rock samples whereas immobile Al<sub>2</sub>O<sub>3</sub> is relatively constant (Table 4). The distribution of major oxides shows that SiO<sub>2</sub> and TiO<sub>2</sub> are enriched in altered granite, while Fe<sub>2</sub>O<sub>3</sub>, MnO, MgO, CaO, Na<sub>2</sub>O, K<sub>2</sub>O, and P<sub>2</sub>O<sub>5</sub> are depleted (Fig. 6a). Altered basalt is enriched in SiO<sub>2</sub>, Na<sub>2</sub>O and K<sub>2</sub>O but depleted in TiO<sub>2</sub>, Fe<sub>2</sub>O<sub>3</sub>, MnO, MgO, CaO, and P<sub>2</sub>O<sub>5</sub>, while K<sub>2</sub>O and P<sub>2</sub>O<sub>5</sub> are enriched in altered trachyte compared to SiO<sub>2</sub>, TiO<sub>2</sub>, Fe<sub>2</sub>O<sub>3</sub>, MnO, MgO, CaO, and Na<sub>2</sub>O, which are depleted. The trace element composition in altered granite show enrichment of Ce, La, Nb, Nd, Y, Th, and Zr against the depletion of Ba, Ga, Rb, Sr and Zn (Fig. 6b). Altered basalt is enriched in Ga, La, Nb, Rb, Th, Zn, and Zr but depleted in Ba, Ce, Nd, Sr, and Y. Altered trachyte show Ba, La, Nd, Th and Y enrichment and Ga, Nb, Sr, Zn and Zr depletion. Clay mineral phases are enriched in Sr, Y, and Zr but depleted in Th and Zn.

#### **4.3. Chemical weathering**

Figure 7 indicates intermediate and strong chemical weathering for clay (Cl) and sandstone (SST), respectively, in the SDLSW. Chemical weathering intensity varied from weak (50-60) for altered granite (AG), altered trachyte (AT) and altered basalt (AB) to strong ( $> 85$  CIA unit) in laterite (LT) at TBIW. According to Andrews et al. (2004), the observed CIA values suggest strong leaching of Ca, Na and K and the formation of kaolinite, illite, and smectite. On stable well-drained land surfaces where weathering and leaching have been prolonged, the oxisols (ferrosols) develop kaolinitic and, in extreme cases gibbsite, the clay minerals identified to be in equilibrium with the sampled water (SM3a-b). Such sites are characterized by iron-rich (laterite) and aluminous (bauxite) surface deposits. Both the laterite, which exists in the watersheds, and bauxite in neighbouring Minim-Martap bauxite-rich watershed (Nyamsari et al., 2017) promote increased runoff in the SDLSW and the TBIW.

From the hypothesis that well-drained landscapes usually result in gibbsite formation and poorly drained soil in kaolinite and smectite development (Vuai et al., 2007), the common presence of gibbsite and kaolinite in the studied watersheds concur with the sandy and lateritic soils in the SDLSW and the TBIW, respectively. These observations point to the excellent and poor drainage capacities of the SDLSW and the TBIW, respectively, as key contributors to their mineralogical compositions. Moreover, intensive mechanical erosion may have partly influenced both the observed weathering rates of 0.00061 mm/yr, 0.0014 mm/yr, 0.00069 mm/yr and 0.0005 mm/yr for the granite, basalt, trachyte and sandstones, respectively (Table 5), and the weathering type that formed gibbsite and kaolinite (Tokashiki, 1993).

#### **4.4. Stoichiometry and dissolved carbonate phases**

The relative abundances (Ab) of albite, 53 mol% for the SDLSW and 61 mol% for the TBIW (Tables 6a-b), is a proxy for the abundance of Na-plagioclases which are dominant. The Na-plagioclase likely to dissolve in the watersheds is the andesine (Ab<sub>50</sub> to Ab<sub>70</sub>). Considering that granite, syenite, basalt, arkosic sandstones and conglomerates are found in the SDLSW, water dissolution of andesine occurs in the upstream igneous rocks, and the downstream arkosic sandstones and conglomerates. In addition, the bivariate plots Mg vs. HCO<sub>3</sub>, Sr vs. HCO<sub>3</sub>, and Ca vs. HCO<sub>3</sub> scatter plots (SM4a-c) show a positive correlation for the water samples from the TBIW and some samples from the SDLSW, suggesting that the local carbonate minerals, dolomite CaMg(CO<sub>3</sub>)<sub>2</sub>, calcite (CaCO<sub>3</sub>) and strontianite (SrCO<sub>3</sub>), dissolve alongside the plagioclases.

#### **4.5. Elemental and chemical fluxes**

Elemental and chemical fluxes follow the trend  $\text{HCO}_3 > \text{Na} > \text{Ca} > \text{SiO}_2 > \text{Fe} > \text{Mg} > \text{Cl} > \text{F} > \text{BO}_2 > \text{Mn} > \text{NH}_4 > \text{Zn} > \text{Al} > \text{Ba} > \text{Sr} > \text{SO}_4 > \text{K}$  in the TBIW, with annual nutrient losses of  $\text{Na} > \text{Ca} > \text{Fe} > \text{Mg} > \text{Cl} > \text{B} > \text{Mn} > \text{N} > \text{Zn} > \text{Al} > \text{S} > \text{K}$ . In the SDWLS, the trend is the following:  $\text{HCO}_3 > \text{SiO}_2 > \text{Na} > \text{Ca} > \text{K} > \text{Mg} > \text{NO}_3 > \text{Cl} > \text{Fe} > \text{Al} > \text{F} > \text{SO}_4 > \text{Zn} > \text{Sr} > \text{Ba} > \text{Mn} > \text{BO}_2 > \text{NH}_4 > \text{PO}_4 > \text{Br} > \text{NO}_2 > \text{Ti}$ , with annual nutrients losses of  $\text{Na} > \text{Ca} > \text{K} > \text{Mg} > \text{N} > \text{Cl} > \text{Fe} > \text{Al} > \text{S} > \text{Zn} > \text{Mn} > \text{B} > \text{PO}_4$ . Comparatively, it is observed that the SDLSW loses more nutrients annually than the TBIW (Fig. 8), because the SDLSW is made of more dissolvable igneous rocks in its upper part.

## 5. DISCUSSION

### 5.1. Rate of chemical weathering

Calculated chemical weathering rates (Table 6) are ca. 10 to 1000 times lower than those reported for crystalline rocks in the Congo Basin (0.0085 to 0.078 mm/yr; Nkounkou and Probst 1987), basalts at Lake Nyos (ca. 5 mm/yr; Fantong et al., 2015), sandstone (0.013 mm/yr) and granitoids in the Nsimi Zoetele tropical forest watershed (2.8 mm/yr) (Braun et al., 2005).

The lower rates of chemical weathering could be attributed to the impermeable and inert characteristics of the lateritic duricrust in the TBIW, which is already a product of strong oxidative weathering. In the SDLSW, they could be attributed to the presence of oxidative weathering products such as hematite-rich ferruginous sandstones and goethite, which increase runoff and shorten water-rock interaction time.

### 5.2. Relative mobility of elements

A zig-zag pattern of relative mobility of elements in the TBIW (Fig. 9a) and the SDLSW (Fig. 9b) suggests non-isochemical dissolution of rocks in the watersheds (Aiuppa et al., 2005). Except for Mo, the nutrients Ca, Mn, Na, Cu, Zn, K and Ni exhibit high relative mobility compared to Cr, Cs, Ga, Pb, Th, Fe, U, V, and Al in both watersheds. Mean mobility sequences for (analysed) alkalis vary as  $\text{Na} > \text{K} > \text{Rb} > \text{Cs}$ , and for (analysed) alkaline earth elements as  $\text{Ca} > \text{Ba}$ . Both sequences are similar to the Hofmeister series for the relative affinity of cations for clay minerals and oxides (Stumm and Morgan, 1996). Thus, water-rock interactions are a controlling factor for the distribution of these elements between the aqueous and solid phases in both watersheds. Mn, Ca, Na, K, Ti, Rb and Cu are among the most mobile elements in the TBIW and the SDLSW. Al has a remarkable immobility, being retained in the products of incongruent dissolution as kaolinite and gibbsite. Contrary to the results in the Benue River

Basin (Fantong et al., 2020), Mo, Cs and Sn are among the least mobile elements in the TBIW and the SDLSW.

### 5.3. Hydrogeochemistry

The maximum EC values in the TBIW (160  $\mu\text{S}/\text{cm}$ ; Table 1) and the SDLSW (698  $\mu\text{S}/\text{cm}$ ; Table 1) differ from the maximum recorded in the shallow aquifers of Lake Chad Basin (8250  $\mu\text{S}/\text{cm}$ ; Huneau et al., 2017), in the Iullemeden aquifer (2700  $\mu\text{S}/\text{cm}$ ; Zouari 2017), and in the Liptako-Gourma hydrological basin (2000  $\mu\text{S}/\text{cm}$ ; Taupin 2017). A similar comparison with pH suggests a shorter groundwater residence time and a lower water-rock interaction intensity in the TBIW and the SDLSW, compared to aquifers in the aforementioned Sahelian hydrological basins. However, the water-rock interaction intensity is strong enough to form secondary clay minerals such as gibbsite and kaolinite and the water types become enriched in Ca+Mg- $\text{NO}_3$  in the SDLSW and Ca+Mg- $\text{HCO}_3$  in the TBIW (SM1b). Although the observed water types are similar to the signatures of some groundwater in the Benue River basin (Fantong et al., 2020; Njitchoua et al., 1997), they do differ significantly from other water types in the Sahelian Taoudeni and Iullemeden shallow aquifers (Ca+Mg- $\text{SO}_4+\text{Cl}$  and Ca- $\text{Cl}+\text{SO}_4$ ), which are influenced by evaporation and salinization (Taupin 2017; Zouari 2017). Sighomnou et al. (2013) have also reported the observed rain and surface water dominant characteristics near Niamey (Niger), where runoff due to hard-crusted soil is common. Comparable to the Benue River Basin (Fantong et al., 2020), a similar silicate (feldspars) - induced REEs pattern is observed, but the REEs do not show preferential concentration in water samples from agricultural lowlands as suggested by Chen et al. (2019) in a granitic watershed in Southern China. Moreover, our results, which shows that Na and K are gained during the chemical weathering of basalt in the TBIW (Fig. 6), contradicts the findings of Etame et al. (2009) who report extensive loss of Na and K from Mt. Etinde volcanic rocks in the equatorial zone of Cameroon. However, there is similarity with the loss of Ba, Sr, Ca, Mg, Rb, Fe, Mn, and Zn, and the gain of La, Ce, Ga, and Zr. The non-isochemical dissolution of rocks (Fig. 9) is in agreement with the results obtained by Fantong et al. (2020) in the Benue River basin, which consists of sedimentary and igneous rocks, and by Aiuppa et al. (2005) at Mt. Vesuvius (volcanic rocks).

### 5.4. Behaviour of $\text{Fe}^{2+}$ , $\text{Mn}^{2+}$ , P and trace elements nutrients

In reducing (anoxic) chemical weathering environments, oxides of iron (Fe) and manganese (Mn) may be reduced to soluble Fe (II) and Mn (II), causing them to be relatively mobile as

observed in the studied watersheds (Fig. 9). Considering that Fe is more soluble under acidic conditions than Mn, and the predominantly acidic conditions in the aquifer (Fig. 3a), Fe (II) should be more mobilised than observed in Figs. 3, 9 and 10c. The weak mobility of Fe could be explained by the following hypothesis: the low concentrations of phosphorus (P) could be linked to trapping of P by Fe hydroxide in the ferruginous soil, making phosphorous unavailable for plant growth. The Fe-rich soil will also strongly bind and remove many key nutrients from solution, including B, Co, Mn, Mo, Ni, Zn, Cu (Fig. 3c-d), thereby reducing crop yield due to the negative impact on photosynthesis. Moreover, P concentration has been reported to vary inversely with river discharge (Andrews et al., 2004), and the data we present in this study are for the rainy season (higher stream discharge), thus P concentrations are expected to be low in shallow groundwater near the low-yield sites as shown in Fig. 10. Such immobility and reduction in Fe concentrations are in agreement with observations made in the volcanic aquifers of Mt. Vesuvius (Aiuppa et al., 2005), Mt. Etna volcano (Aiuppa et al., 2000), and Mt. Etinde, where Fe immobility is caused by re-precipitation of Fe-hydroxides (Etame et al., 2009), commonly present in the duricrust that abounds in the studied watersheds.

#### **5.5. Contrasting behaviour of $\text{NO}_3^-$ and REEs in the two watersheds**

The higher concentration of  $\text{NO}_3$  (ca. 20 times) in the SDLSW compared to the TBIW (Fig. 3a-b) is attributed to agricultural practices in the SDLSW where the use of NPK fertilizers is more common than in the TBIW. The  $\text{NH}_4$ -rich waste and N-rich fertilizers are later transformed into easily oxidized  $\text{NO}_3$ . Such mechanisms of  $\text{NO}_3$  enrichment in shallow groundwater are common in other Sahelian watersheds (Fantong et al., 2010, Huneau et al., 2017, and Bello et al., 2018) characterized by anthropogenic inputs.

The higher fractionation of REEs in the SDLSW compared to the TBIW (Fig. 5) could be due to either a longer residence time of water circulating in the SDLSW (ca. 10 times larger and with a gentler topography), or to surface waters containing more oxygen which promotes the precipitation of Mn and Fe oxides from the surface waters into the aquifers. These oxides will then bind and release REEs in the deeper anoxic settings as they dissolve. The difference in the physiographic features and geology between the two watersheds also influences the variability of elemental fluxes, with lower fluxes in the TBIW than in the SDLSW (Fig. 8).

#### **5.6. Nutrients and REEs of waters at sites with low yields**

To assess nutrient and REEs contents based on water chemistry, average concentrations from the shallow groundwater in dug wells near low-yield sites were further analysed (Fig. 10). For

all sites, shallow groundwater contains very low concentration of  $\text{PO}_4^{3-}$  (Fig. 10a),  $\text{Fe}^{2+}$  (Fig. 10b), and Mo (Fig. 10c), indicating that their poor soil nature could be due partly to the lack of phosphorus, iron, and molybdenum.

$\text{NO}_3^-$  (Fig. 10a),  $\text{K}^+$  (Fig. 10b), Bo (Fig. 10c) and REEs (Fig. 10d) show deficiency at sites S4, S5, and S6 (TBIW), compared to excess of  $\text{NO}_3^-$ ,  $\text{K}^+$ ,  $\text{Ca}^{2+}$ , Mn and REEs at sites S1, S2, S3 (SDLSW).

Shallow groundwater in the TBIW sites is poor in nutrients and REEs compared to the SDLSW sites. The low REEs concentrations in the TBIW contradict the hypothesis from Chen et al. (2019) that concentrations of LREEs and HREEs increase in granitic watersheds in Southern China.

## 6. CONCLUSIONS AND RECOMMENDATIONS

Weak to strong chemical weathering of rocks in the TBIW and SDLSW causes incongruent and non-isochemical dissolution of silicates and carbonates. The chemical weathering, which decomposes the rocks at faster rates in the TBIW relative to the SDLSW, is lower than for crystalline rocks, basalts and sandstones. With the exception of Mo, the elements Ca, Mn, Na, Cu, Zn, K, Ni, and Fe show a greater mobilization pattern during chemical weathering than non-essential trace elements, Cr, Bi, Cs, Cu, Ga, Pb, Sn, Th, U, V and Al. In both watersheds, the most mobilized elements are Mn, Ca, Na, K, Ti, Rb and Cu, with  $\text{Na} > \text{K} > \text{Rb}$  in descending order for the alkalis and  $\text{Ca} > \text{Ba}$  for the alkaline earth elements. Contributions from water-rock interaction and elemental mobilities characterize the groundwater that originates from rainwater to have a  $\text{Ca}+\text{Mg}-\text{NO}_3$  signature in the anthropic-impacted SDLSW and  $\text{Ca}+\text{Mg}-\text{HCO}_3$  signature from the influence of plagioclases dissolution in the TBIW. Elemental fluxes and annual losses of nutrients are higher in the larger gentle sloping SDLSW than in the smaller and steeper TBIW.

Based on water chemistry, low-yield soil sites could be caused by: (1) co-precipitation of phosphorus and iron to form insoluble  $\text{PO}_4$ -rich iron hydroxide (Fe and P) sink leading to P and Fe deficiencies in both watersheds; (2) deficiency in N, K, B, and REEs in the TBIW; (3) excess of N, K, Ca, Mn, and REEs in the SDLSW.

Water retention infrastructures should be constructed at selected locations in both watersheds to prevent nutrient losses. The nutrient content of soil in the TBIW may be augmented with N, K, B and REEs external inputs, while the application of nitrogenous fertilizers in the SDLSW

soil should be regulated to ensure the concentrations of N, K, Ca, Mn, and REEs to stay below recommended levels. Our study provides a hydrogeochemical modelling of nutrient cycling in two watersheds in northern Cameroon, with wider implications for agricultural practices across the Sahel microclimatic regions, if it is coupled with studies on nutrients content in soils and plants.

## Captions of Figures

Fig. 1. Location of selected watersheds, (a) within the Sahel belt of Africa, and (b) within Cameroon. Simplified geological maps of (c) the Sahel Douka Longo Sedimentary Watershed (SDLSW), and (d) the Transitional Bidou Igneous Watershed (TBIW). Locations of water sampling sites, hydrometric stations, and sites of soils with low yields are also shown for both watersheds.

Fig. 2. Typical weathering structures: (a) Decimetric “sandstone balls”, (b and c) with conglomerate core and sandstone crust. (d) In some locations, a mosaic of potholes represents relics of the coarser conglomerate cores that have been differentially weathered.

Fig. 3. Variations of mean concentrations in groundwater and surface water: major ions (a) in the SDLSW, and (b) in the TBIW, as well as trace elements (c) in the SDLSW, and (d) in the TBIW.

Fig. 4. PAAS normalized patterns of rare-earth elements (REEs) in the water samples. For clarity, the data are shown with three subplots for the TBIW (a-c) and four sub-plots for the SDLSW (d-g). All samples show a conspicuous “steep roof-shaped” positive Eu anomaly.

Fig. 5. Mean concentrations for groundwater and surface water of (a) LREEs and (b) HREEs in the SDLSW, and respectively (c) and (d) in the TBIW.

Fig. 6. Enrichment and depletion of (a) major-element oxides and (b) trace elements, after chemical weathering of rocks in the watersheds.

Fig. 7. Classification of rocks chemical weathering: correlation between the CIA and PI in fresh basalt (FB), altered basalt (AB), fresh granite (FG), altered granite (AG), fresh trachyte (FT), altered trachyte (AT), clay (Cl), sandstone (SST), and laterite (LT) sample from the watersheds.

Fig. 8. Calculated elemental and chemical fluxes in the two watersheds.



Fig. 9. Relative mobility (RM) of elements in selected water samples in (a) TBIW and (b) the SDLSW (b). RM values were normalized to magnesium and computed from equation (12) (see text).

Fig. 10. Mean concentrations in shallow groundwater near the poor crop yield sites: (a) major anion nutrients, (b) major cation nutrients, (c) trace element nutrients, and (d) REEs. Sites S1, S2, and S3 are in the SDLSW, while S4, S5, and S6 are in the TBIW.

## Table Captions

Table 1. Statistical summary of major ions, nutrients, SiO<sub>2</sub>, stable environmental isotopes, and pCO<sub>2</sub> of groundwater (n = 36) and surface water (n = 16) sampled during the rainy season in the TBIW (n = 34) and the SDLSW (n = 25).

Table 2. Statistical summary of trace element concentrations in groundwater and surface water sampled during the rainy season in the TBIW and the SDLSW.

Table 3. Statistical summary of rare Earth elements content in groundwater and surface water sampled during the rainy season in the TBIW and in the SDLSW.

Table 4. Calculated chemical weathering rates for granite, basalt, trachyte and sandstone samples from the watersheds.

Table 5a. Calculated values (weight %) for the minerals (albite, K-feldspars, biotite, anorthite, gypsum, and halite) dissolved in a litre of water in the SDLSW.

Table 5b. Calculated values (weight %) for the minerals (albite, K-feldspars, biotite, anorthite, gypsum, and halite) dissolved in a litre of water in the TBIW.

## Acknowledgements

This study was funded by the Federal Ministry for Economic Cooperation and Development (BMZ) - Germany (BMZ No. 2016.2034.3), as part of the ProSEP project in Cameroon. This specific study was implemented by the Federal Institute of Geoscience and Natural Resources

(BGR) - Germany (BGR No. 05-2397), and the Institute of Geological and Mining Research (IRGM), Yaoundé. The authors would like to thank their colleagues at the BGR (Dr Paul Königer and Frank Korte among others) who carried out the lab analyses and/or helped to complete the method section. We are thankful to Dr. Robert Kringel (BGR) for his comments that improved the quality of the manuscript as well as two anonymous reviewers for their meaningful comments.

## REFERENCES

- Adomako D., Gibrilla A., Maloszewski P., Ganyaglo S. Y., and Rai S. P. (2015) Tracing stable isotopes ( $\delta^2\text{H}$  and  $\delta^{18}\text{O}$ ) from meteoric water to groundwater in the Densu River basin of Ghana. *Environmental Monitoring and Assessment*, 187, 264. <https://doi.org/10.1007/s10661-015-4498-2>
- Aiuppa A., Allard P., D'Alessandro W., Michel A., Parello F., Trueil M., et al. (2000) Mobility and fluxes of major, minor and trace metals during basalt weathering and groundwater transport at Mt. Etna volcano (Sicily). *Geochemica et Cosmochimica Acta*, 64(11), 1827–1841.

769 Aiuppa A., Federico C., Allard P., Gurrieri S., and Valenza M. (2005) Trace metal modelling  
 770 of groundwater-gas-rock interactions in a volcanic aquifer: Mount Vesuvius, Southern  
 771 Italy. *Chemical Geology*, 216, 289–311.

772 Andrews J. E., Brimblecombe P., Jickells T. D., Liss P. S., and Reid B. J. (2004) An  
 773 Introduction to Environmental Chemistry. Blackwell Publishing. Oxford-UK. 2<sup>nd</sup>  
 774 Edition. 296 pp.

775 Asai K., Satake H., and Tsujimura M. (2010) Isotopic approach to understanding the  
 776 groundwater flow system within the andesitic strato-volcano in a temperate humid  
 777 region: case study of Ontake volcano, Central Japan. *Hydrological Processes*, 23, 559–  
 778 571.

779 Bello M., Ketchemen-Tandia B., Nlend B., Huneau F., Fouepe A., Fantong W.Y., Ngo Boum-  
 780 Nkot S., Garel E., Celle-Jeanton H. (2019) Shallow groundwater quality evolution after  
 781 20 years of exploitation in the southern Lake Chad: hydrochemistry and stable isotopes  
 782 survey in far north of Cameroon. *Environmental Earth Sciences* 78:474.  
 783 <http://doi.org/10.1007/s12665-019-8494-7>.

784 Birke M., Reimann C., Demetriades A., Rauch U., Lorenz H., Harazim B., et al. (2010)  
 785 Determination of major and trace elements in European bottled mineral water—  
 786 analytical methods. *Journal of Geochemical Exploration*, 107, 217–226.  
 787 <https://doi.org/10.1016/j.gexplo.2010.05.005>.

788 Boeglin J.-L., and Probst J.-L. (1998) Physical and chemical weathering rates and CO<sub>2</sub>  
 789 consumption in a tropical lateritic environment; The upper Niger basin. *Chem. Geol.*  
 790 148, 137-157.

791 Bowen N. L., (1928) The evolution of the igneous rocks. Princeton Univ. Press

792 Brand W. A., et al. (2009) Cavity ring-down spectroscopy versus high temperature conversion  
 793 isotope ratio mass spectrometry; a case study on  $\delta^2\text{H}$  and  $\delta^{18}\text{O}$  of pure water samples  
 794 and alcohol/water mixtures. *Rapid Communication in Mass Spectrometer*, 23, 1879-  
 795 1884. <https://doi.org/10.1002/rcm.4083>.

796 Braun J.-J., Ndam J. R. N., Viers J., Dupre B., Bedimo J. P., Boeglin J.-L., Robain H., Nyeck  
 797 B., Freydier R., Nkamdjou L. S., Rouiller J., and Muller J.-P. (2005) Present weathering

798 rates in a humid tropical watershed: Nsimi, South Cameroon. *Geochimica et*  
799 *Cosmochimica Acta*, 69, No. 2, pp. 357–387.

800 Brimhall G. H. and Dietrich W. E. (1987) Constitutive mass balance relations between  
801 chemical composition, volume, density, porosity, and strain in metasomatic  
802 hydrochemical systems: results on weathering and pedogenesis. *Geochim. Cosmochim.*  
803 *Acta* 51, 4419-4434.

804 Bruijnzeel L. A. (1990) Hydrology of moist tropical forests and effects of conversion: a state  
805 of knowledge review. International Hydrological Programme-Humid Tropics  
806 Programme. UNESCO.

807 Chabejong N. E. (2016) A review on the impact of climate change on food security and  
808 malnutrition in the Sahel Region of Cameroon. In: Leal Filho W., Azeiteiro U., Alves F.  
809 (eds) *Climate Change and Health. Climate Change Management*. Springer, Cham. DOI:  
810 10.1007/978-3-319-24660-4\_9

811 Chen H., Chen Z., Chen Z., Ma Q., Zhang Q. (2019) Rare earth elements in paddy fields from  
812 eroded granite hilly land in a southern China watershed. *PLoS ONE* 14(9): e0222330.  
813 [https:// doi.org/10.1371/journal.pone.0222330](https://doi.org/10.1371/journal.pone.0222330).

814 Cheo, A. E., Voigt, H. J., & Mbua, R. L. (2013). Vulnerability of water resources in northern  
815 Cameroon in the context of climate change. *Environmental Earth Sciences*, 70(3), 1211-  
816 1217.

817 Cotten J., Le Dez A., Bau M., Maury R. C., Dulski P., Fourcade S., Bohn M., Brousse. (1995)  
818 Origin of anomalous rare earth element and yttrium enrichments in subaerially exposed  
819 basalts: evidence from French Polynesia. *Chem. Geol.* 119, 115-138.

820 Craig H. (1961) Isotopic variations in meteoric waters. *Science* 133:1702-1703.

821 Dalai T. K., Krishnawami S., Sarin M. M. (2002) Major ion chemistry in the headwaters of the  
822 Yamuna river system: Chemical weathering, its temperature dependence and CO<sub>2</sub>  
823 consumption in the Himalaya. *Geochim. Cosmochim. Acta* 66, 3397-3416.

824 Dassou E. F., Ombolo A., Chouto S., Mboudou G. E., Abate Esse J. M., Benili E. (2016) Trends  
825 and geostatistical interpolation of Spatio-Temporal variability of precipitation in  
826 Northern Cameroon. *American Journal of Climate Change*, 5: 229-244.

827 Dehnavi, A. G., Sarikhani, R., & Nagaraju, D. (2011). Hydro geochemical and rock water  
828 interaction studies in East of Kurdistan, NW of Iran. *Int J Environ Sci Res*, 1(1), 16-22.

829 Drever J. I. and Clow D. W. (1995) Weathering rates in catchments. In *Chemical Weathering*  
830 *Rates of Silicate Minerals*, Vol. 31 (ed. A. F. White and S. L. Brantley), pp. 463–483,  
831 Mineralogical Society of America.

832 Edet A. E. (2004) A preliminary assessment of the concentrations of rare earth elements in an  
833 acidic fresh groundwater (south-eastern Nigeria). *Applied Earth Science*, 113, 100-109.

834 Elderfield H. and Greaves M. J. (1982) The rare earth element elements in seawater. *Nature*,  
835 296, 214-219

836 Epule T. E., Ford J. D., Lwassa S. (2018) Climate change stressors in the Sahel. *GeoJournal*  
837 83:1411-1424

838 Etame J., Gerard M., Bilong P., Suh C. E. (2000) Behaviour of elements in soils developed  
839 from nephelinites at Mount Etinde (Cameroon): Impact of hydrothermal versus  
840 weathering processes. *Journal of African Earth Sciences*. 54, 37- 45.

841 Fantong W. Y. (2010) Hydrogeochemical and Environmental Isotopic Study of Groundwater  
842 in Mayo Tsanaga River Basin, Northern Cameroon: Implication for Improving Public  
843 Groundwater Supply Management. Ph.D. Thesis. The Graduate School of Science and  
844 Engineering for Education, University of Toyama, Japan. 187 pp.

845 Fantong W. Y., Kamtchueng B. T., Yamaguchi K., Ueda A., Issa N. R., Wirmvem M. J., et al.  
846 (2015) Characteristics of chemical weathering and water–rock interaction in Lake Nyos  
847 dam (Cameroon): Implications for vulnerability to failure and re-enforcement. *Journal*  
848 *of African Earth Sciences*, 101, 42-55.

849 Fantong W. Y., Kamtchueng B. T., Ketchemen-Tandia B., Kuitcha D., Ndjama J., Fouepe, A.  
850 T., et al. (2016). Variation of hydrogeochemical characteristics of water in surface  
851 flows, shallow wells, and boreholes in the coastal city of Douala (Cameroon). *Hydrol:*  
852 *Science Journal*. <https://doi.org/10.1080/0262666720161173789>.

853 Fantong W. Y., Nenkam Therese L. L. J., Nbandah P., Kimbi S. B., et al. (2020) Compositions  
854 and mobility of major,  $\delta D$ ,  $\delta^{18}O$ , trace, and REEs patterns in water sources at Benue River  
855 Basin-Cameroon: implications for recharge mechanisms, geo-environmental controls and  
856 public health. *Environ. Geochem. Health*. 42, 2975-3013.

857 Fantong W. Y., Satake H., Aka F. T., Ayonghe S. N., Asai K., Mandal A. (2010)  
 858 Hydrochemical and isotopic evidence of recharge, apparent age, and flow direction of  
 859 groundwater in Mayo Tsanaga River Basin, Cameroon: Bearings on contamination.  
 860 Environmental Earth Sciences, 60, 107-120.

861 Faure G. (1991) Principles and applications of inorganic geochemistry (p. 626). New York:  
 862 Macmillan Publishing.

863 Feth J. H., Roberson C. E., and Polzer W. L. (1964) Sources of mineral constituents in water  
 864 from granitic rocks, Sierra Nevada, California and Nevada. U.S. Geol. Surv. Water-  
 865 Supply Paper, 1535-I.

866 Forth H. D. (1984) Fundamentals of Soil Science, 7<sup>th</sup> ed. Wiley, New York, 435 pp.

867 Garrels R. M., and Mackenzie F. T. (1967) Origin of the chemical composition of some springs  
 868 and lakes. In R. F. Gould (Ed.), Equilibrium concept in natural water systems (pp. 222-  
 869 242). Washington, DC: American Chemical Society.

870 Gat J. R. (2010) Isotope hydrology: A study of the water cycle (Vol. 6)., Series on  
 871 environmental science and management London: Imperial College Press.

872 Gislason S. R., Arnorsson S., and Armannsson H. (1996) Chemical weathering of basalts in  
 873 southwest Iceland: Effects of runoff, age of rocks and vegetative/glacial cover.  
 874 American Journal of Science, 296, 837–907.

875 Goni I. B. (2006) Tracing stable isotope values from meteoric water to groundwater in the  
 876 south western part of the Chad basin. Hydrogeology Journal, 14, 4331- 4339.

877 Hausrath, E. M., Neaman, A., & Brantley, S. L. (2009). Elemental release rates from dissolving  
 878 basalt and granite with and without organic ligands. *American journal of science*,  
 879 309(8), 633-660.

880 He H., Fan C., Peng Q., Wu M., Zheng J., Gao -Lin Wu G.-L. (2019) Bioaccumulation and  
 881 translocation of rare earth elements in two forage legumes grown in soils treated with  
 882 coal fly ash. Chem. Geol. <http://doi.org/10.1016/j.chemgeo.2019.119284>.

883 Hill I. G., Worden R. H., Meighan I. G. (2000) Yttrium: the immobility-mobility transition  
 884 during basaltic weathering. Geology, 28 (10), 923-926.

885 Hoyle J., Elderfield H., Gledhill A., and Greave M. (1984) The behaviour of the rare earth  
886 elements during the mixing of river and seawaters. *Geochim. Cosmochim. Acta*, 48,  
887 143-149.

888 Huneau F., Abdelkarim A. M. A., Hachim M. S., Tandia B. K., Fantong W. Y., et al. (2017)  
889 Lake Chad Basin. In: *Integrated and Sustainable Management of Shared Aquifer*  
890 *Systems and Basins of the Sahel Region*. Report of the IAEA-supported Regional  
891 Technical Cooperation Project RAF/7/011. Reproduced by the IAEA. Vienna Austria.

892 IRAD. (2018) Tendencies of soil agricultural yields in sub-catchments of Ngaoundere III and  
893 Douka Longo, Cameroon. Internal report in IRAD. 25 pages.

894 Jokam Nenkam, T. L., Kringel, R., Fantong, W. Y., Nbandah, P., Fouépé Takoundjou, A.,  
895 Elisabeth, Z., & Kamtchueng, B. T. (2022). Hydrochemistry of nutrients in  
896 groundwater under farmland in the Benue River Basin, North-Cameroon.  
897 *Environmental Earth Sciences*, 81(7), 1-22.

898 Kebede S., Travi Y., Alemayehu T., and Ayenew T. (2005) Groundwater recharge, circulation  
899 and geochemical evolution in the source region of the Blue Nile River, Ethiopia.  
900 *Applied Geochemistry*, 20, 1658-1676.

901 Kendall C. and Doctor D. H. (2011) Stable isotope applications in hydrologic studies. In H. D.  
902 Holland & K. K. Turekian (Eds.), *Isotope geochemistry* (1st ed., pp. 181-220). London:  
903 Academic Press.

904 Kringel R., Rechenburg, A., Kuitcha, D., Fouépé Takounjou, A., Bellenberg, S. & Kengne, I.,  
905 M. (2016) Mass balance of nitrogen and potassium in urban groundwater in Central  
906 Africa, Yaoundé-Cameroon. *Science of the Total Environment* 547, 382–395.

907 Lis G., Wassenaar L. L., and Hendry M. J. (2008) High precision laser spectrometry D/H and  
908  $^{18}\text{O}/^{16}\text{O}$  measurements of microliter natural water samples. *Analytical Chemistry*, 80,  
909 287-293. <https://doi.org/10.1021/ac701716q>.

910 Little M. G. and Aeolus Lee C.-T. (2006) On the formation of an inverted weathering profile  
911 on Mount Kilimanjaro, Tanzania: buried paleosol or groundwater weathering? *Chem.*  
912 *Geol.* 235, 205-221.

913 Louvat P. (1997) Etude geochemique de l'érosion fluviale des iles volcaniques: l'aide des  
914 bilans d'elements majeurs et traces. These de doctorat: Universite Paris VII.

915 McLennan S. M. (1989) Rare earth elements in sedimentary rocks; influence of provenance  
 916 and sedimentary processes. In B. R. Lipin & G. A. McKay (Eds.), *Geochemistry and*  
 917 *mineralogy of rare earth elements. Reviews in mineralogy and geochemistry* 21 (pp.  
 918 169-200). Chantilly: Mineralogical Society of America.

919 Meybeck M. (1997) Global chemical weathering of surficial rocks estimated from river  
 920 dissolved loads. *American Journal of Science*, 287, 401–428.

921 Migaszewski Z. M., Gałuszka A., & Migaszewski. (2014) The study of rare earth elements in  
 922 farmer's well waters of the Podwis'nio'wka acid mine drainage area (south-central  
 923 Poland). *Environmental Monitoring and Assessment*, 186, 1609-1622.

924 Moldan B. and Cerny J. (1994) Biogeochemistry of small catchments - a tool for environmental  
 925 research. In *Scientific Committee on Problems of the Environment (SCOPE)*, Vol.  
 926 SCOPE 51. Wiley.

927 Molua E. L. (2006) Climatic trends in Cameroon: implications for agricultural management.  
 928 *Climatic Research*, 30, 255-262.

929 Nesbitt H. W. and Wilson R. E. (1992) Recent chemical weathering of basalts. *Am. J. Sci.* 292  
 930 (10), 740-777.

931 Nisha, B. K., Balakrishna, K., Udayashankar, H. N., & Manjunatha, B. R. (2021). Chemical  
 932 weathering and carbon dioxide consumption in a small tropical river catchment,  
 933 southwestern India. *Aquatic Geochemistry*, 27(3), 173-206.

934 Njitchoua R., Aranyossy J. F., Fontes J. C., Michelot J. L., Naah E., Zuppi G. M. (1995)  
 935 Oxygen-18, deuterium et chlorures dans les precipitations à Garoua (Nord-Cameroon):  
 936 implications meteorologiques. *CR Acad Sci Paris*, t 321, serie IIa: 853-860.

937 Njitchoua R., Dever L., Fontes J.-C., & Naah E. (1997). Geochemistry, origin and recharge  
 938 mechanisms of groundwaters from the Garoua Sandstone aquifer, northern Cameroon.  
 939 *Journal of Hydrology*, 190, 123–140.

940 Nkounkou R. R. and Probst J. L. (1987) Hydrology and geochemistry of the Congo river  
 941 system. *Mitt. Geol.-Paleontol. Inst. Univ. Hamb.*, vol. 64. Scope/UNEP, pp. 483-508.

942 Noak C. W., Dzombak D. A., & Karamalidis A. K. (2014) Rare earth element distributions and  
 943 trends in natural waters with a focus on groundwater. *Environmental Science and*  
 944 *Technology*, 48, 4317-4326.



945 Nyamsari, D. G., & Yalcin, M. G. (2017). Statistical analysis and source rock of the Minim-  
 946 Martap plateau bauxite, Cameroon. *Arabian Journal of Geosciences*, 10(18), 1-16.

947 Paces T. (1983) Rate constants of dissolution derived from the measurements of mass balance  
 948 in hydrological catchments. *Geochim. Cosmochim. Acta* 47, 1855–1863.

949 Parker A. (1970) An index of weathering for silicate rocks. *Geol. Mag* Nov. 501-504.

950 Patino L. C., Velbel, M. A., Price J. R., Wade J. A. (2003) Trace element mobility during  
 951 spheroidal weathering of basalts and andesites in Hawaii and Guatemala. *Chem. Geol.*  
 952 202, 343-364.

953 Piper A. M. (1944) A graphic procedure in the geochemical interpretation of water analyses.  
 954 *Am Geophys Union Trans* 25:914 - 923.

955 Price R. C., Gray C. M., Wilson R. E., Frey F. A., Taylor S. R. (1991) The effects of weathering  
 956 on REE, Y and Ba abundances in Tertiary basalts from south-eastern Australia. *Chem.*  
 957 *Geol.* 93, 245-265.

958 Quantin P., Balesdent J., Bouleau A., Delaune M., and Feller C. (1991) Premiers stades  
 959 d'altération de ponces volcaniques en climat tropical humide (Montagne Pelee,  
 960 Martinique). *Geoderma* 50, 125-265.

961 Siegel D. I. and Pfannkuch H. O. (1984) Silicate dissolution influence on Filson Creek  
 962 chemistry, northeastern Minnesota. *Geol. Soc. of Am. Bull.* 95, 1446–1453.

963 Sighomnou D. (2004). Analyse et redéfinition des régimes climatique et hydrologiques au  
 964 Cameroun: Perspective d'évolution des ressources en eaux. Thèse de Doctorat d'état,  
 965 Université de Yaoundé I

966 Stumm W. and Morgan J. J. (1996) Aquatic chemistry: Chemical equilibria and rates in natural  
 967 waters. New Jersey: Wiley.

968 Tardy Y. (1971) Characterization of the principal weathering types by the geochemistry of  
 969 waters from some European and African crystalline massifs. *Chemical Geology*, 7, 253-  
 970 271.

971 Taupin J D., Moulla A. S., Smati A., Komi R. A. K., Galbane A., Kone S., Thiam A., Hmeyade  
 972 B. L., Baca S. D. (2017) Report of the IAEA-supported Regional Technical  
 973 Cooperation Project RAF/7/011. Taoudeni Basin. In Integrated and Sustainable

974 Management of Shared Aquifer Systems and Basins of the Sahel Region. Reproduced  
975 by the IAEA. Vienna Austria. 120 pp

976 Taylor R. G. and Howard K. W. F. (1996) Groundwater recharge in the Victoria Nile basin of  
977 East Africa: support for the soil moisture balance method using stable isotope and flow  
978 modelling studies. *Journal of Hydrology*, 180, 31-53.

979 Thomas M. F. (1994) *Geomorphology in the Tropics. A Study of Weathering and Denudation*  
980 *in Low Latitudes*. John Wiley & Sons.

981 Tokashiki Y. (1993) Soil Survey. 1) Jahgaru, Shimajiri Mahji, Feichisya, Kunigami Mahji. In:  
982 Hirayama, R., Yamada, I. (Eds.), *Soil and Nature of Okinawa Main Island*. Japanese  
983 Society of Pedology, pp. 63-88 (in Japanese).

984 Tsujimura M., Abe Y., Tanaka T., Shimade J., Higuchi S., Yamanaka T., Davaa G., Oyunbaatar  
985 D. (2007) Stable isotopic and geochemical characteristics of groundwater in Kherlin  
986 River Basin: a semiarid region in Eastern Mongolia. *J Hydrol* 333:47-57.

987 Vuai S. A. H. and Tokuyama A. (2007) Solute generation and carbon dioxide consumption  
988 during silicate weathering under sub-tropical humid climate, Northern Okinawa Island,  
989 Japan. *Chem. Geol.* 236, 199-216.

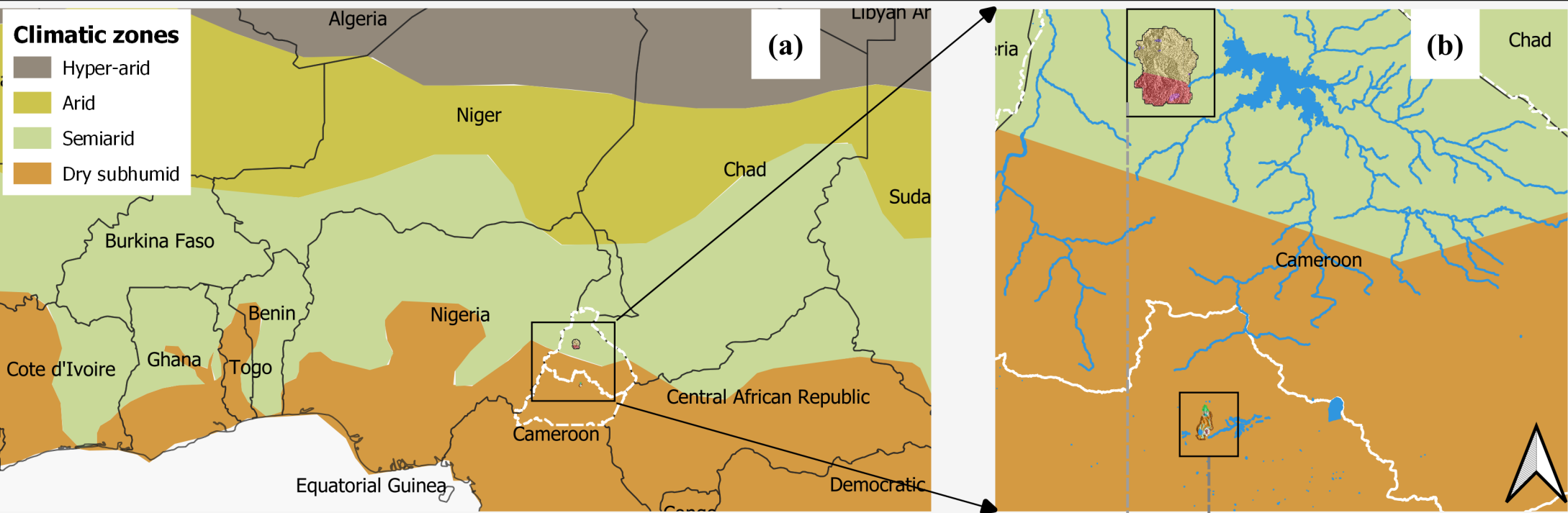
990 White A. F. and Brantley S. L. (1995) Weathering rates of silicate minerals: an overview. In  
991 *Chemical Weathering Rates of Silicate Minerals*, Vol. 31. (eds. White A. F. and Brantley  
992 S. L.), Mineralogical Society of America, pp. 1–21.

993 White A. F., Blum A. E., Bullen T. D., Vivit D. V., Schulz M., and Fitzpatrick J. (1999) The  
994 effect of temperature on experimental and natural chemical weathering rates of granitoid  
995 rocks. *Geochim. Cosmochim. Acta* 63, 3277–3291.

996 White A. T. and Blum A. E. (1995) Effects of climate on chemical weathering in watersheds.  
997 *Geochim. Cosmochim. Acta* 59, 1729– 1747.

998 Zouari K., Moulla A. S., Smati A., Adjomayi P. A., et al. (2017) Report of the IAEA-supported  
999 Regional Technical Cooperation Project RAF/7/011. Iullemeden Aquifer systems. In  
1000 *Integrated and Sustainable Management of Shared Aquifer Systems and Basins of the*  
1001 *Sahel Region*. Reproduced by the IAEA. Vienna-Austria.

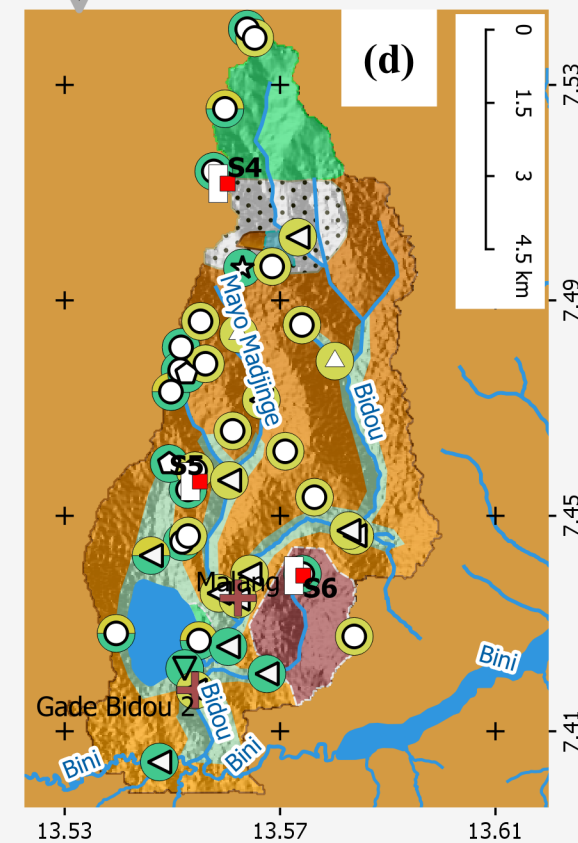
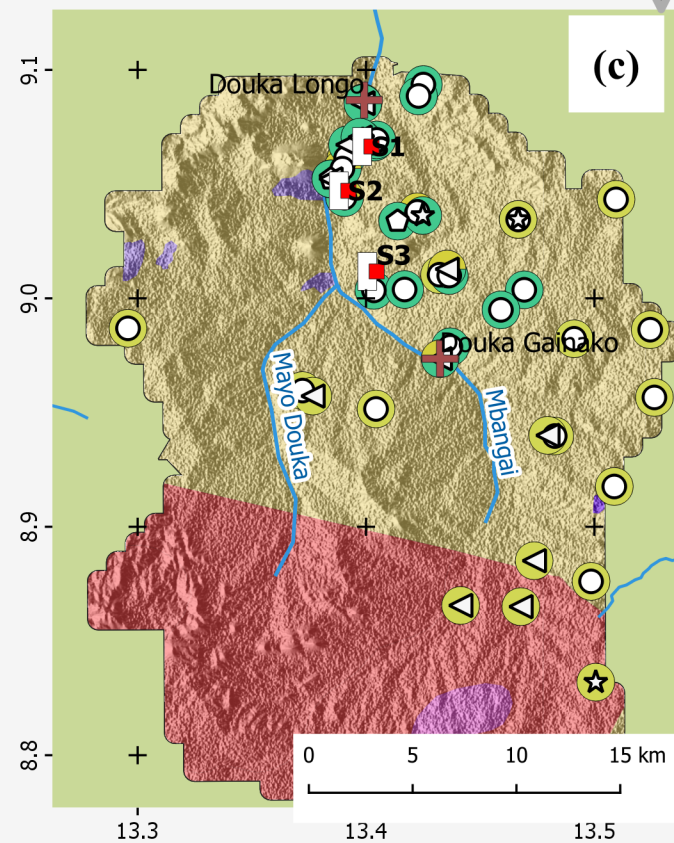
1003  
1004  
1005  
1006  
1007  
1008  
1009  
1010  
1011  
1012  
1013  
1014  
1015  
1016  
1017  
1018



Data sources :

- Cameroon boundaries and river network (OSM, 2018)
- Geological map of Cameroonia West (1959) and geological map of Cameroonia East (1962)
- Climatic zones (Millennium Ecosystems assessment, 2003)

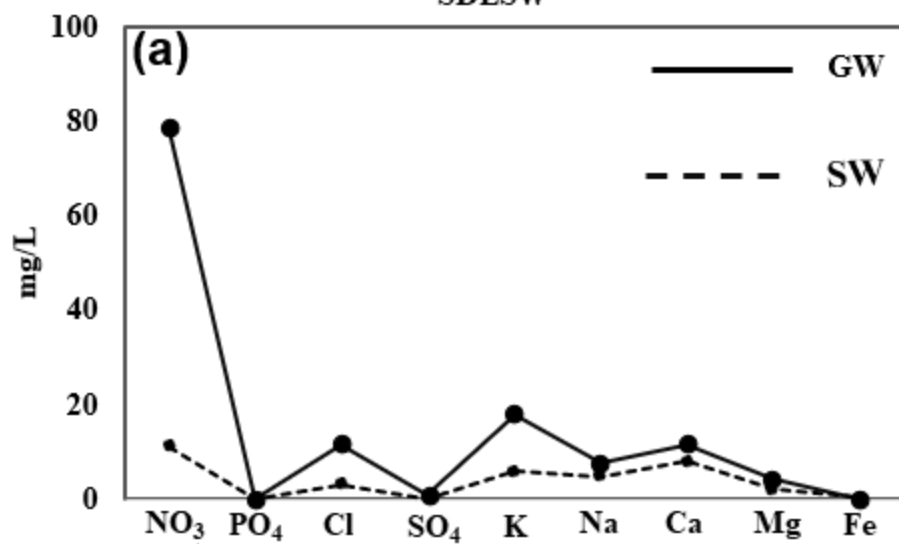
CRS: WGS 84/ EPSG 4326



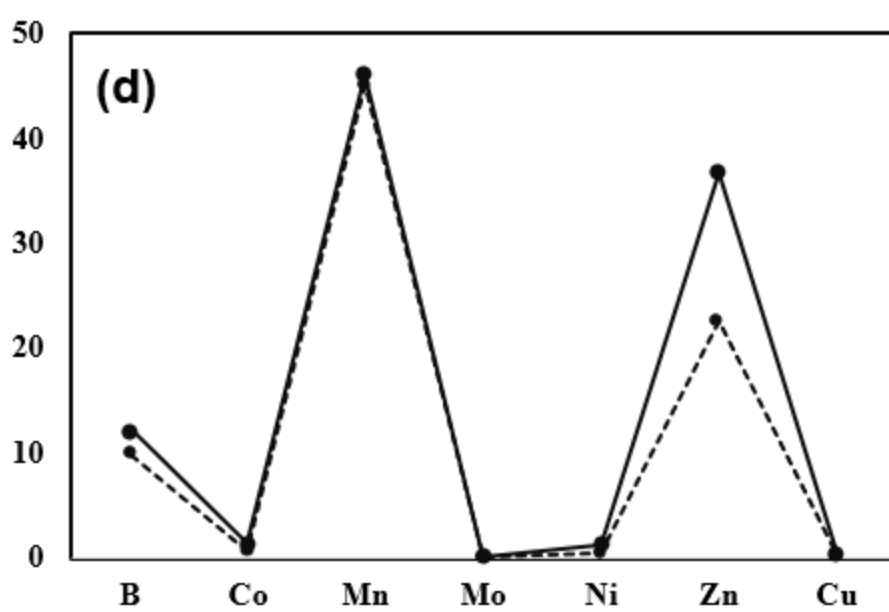
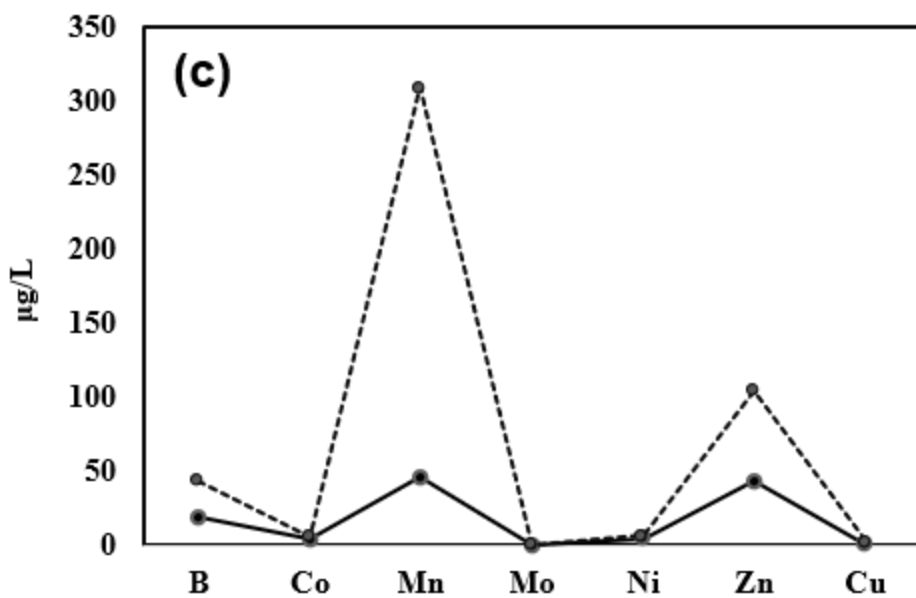
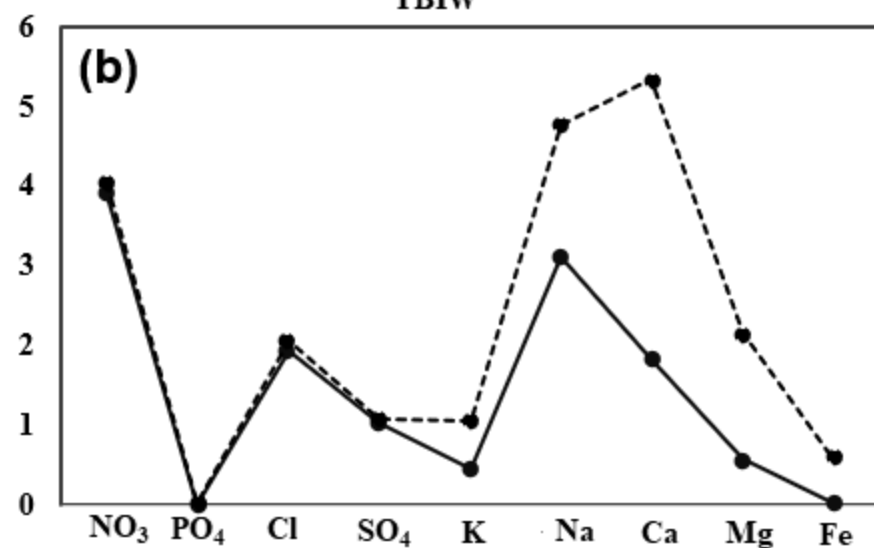




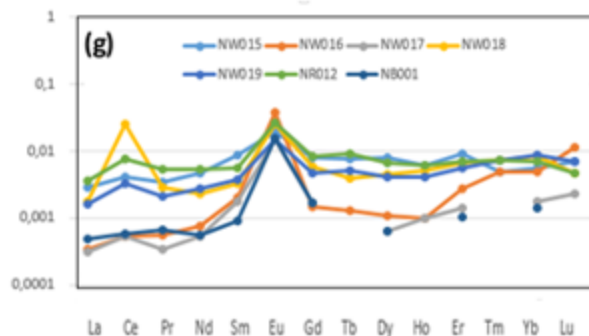
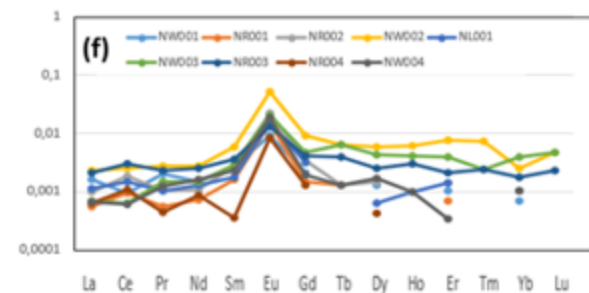
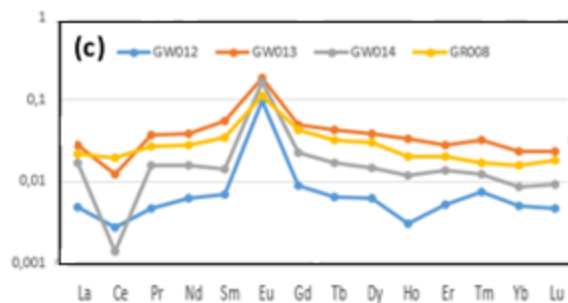
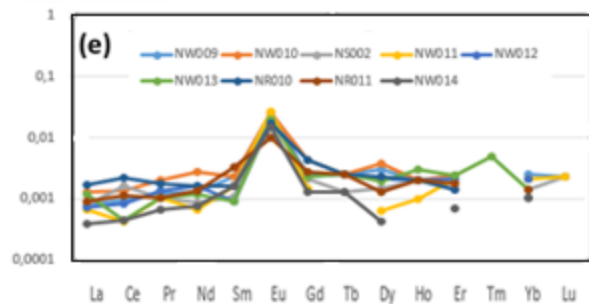
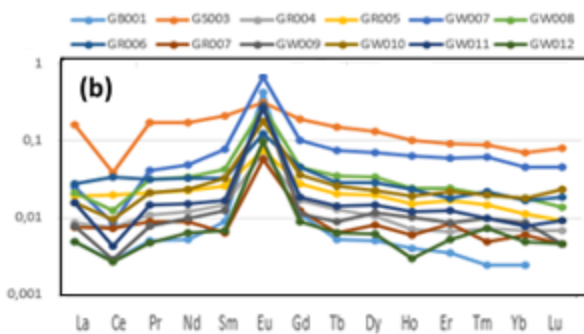
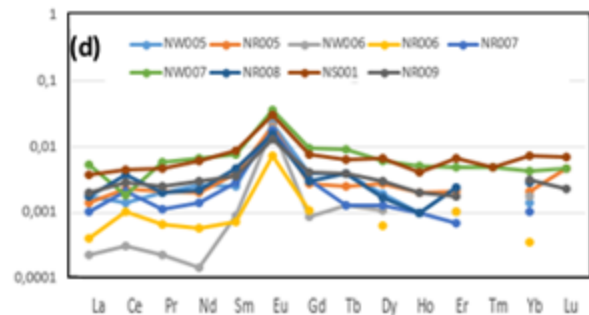
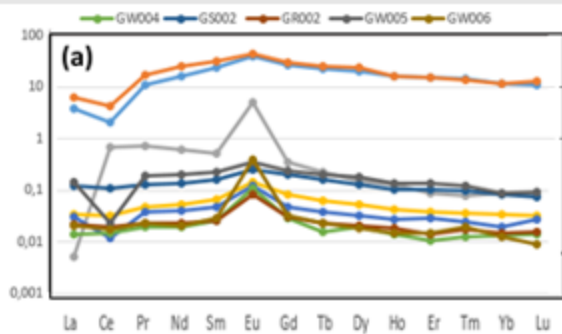
SDLSW

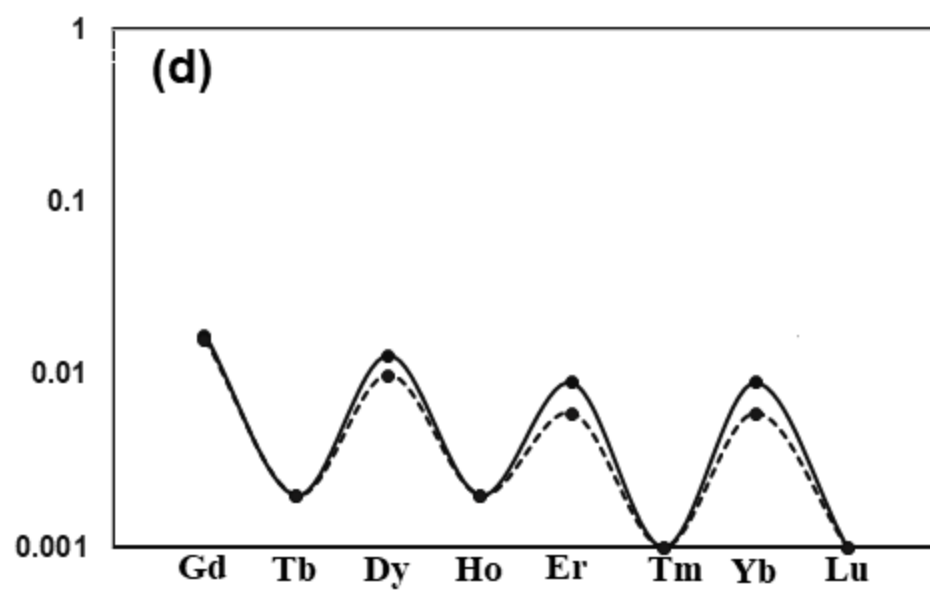
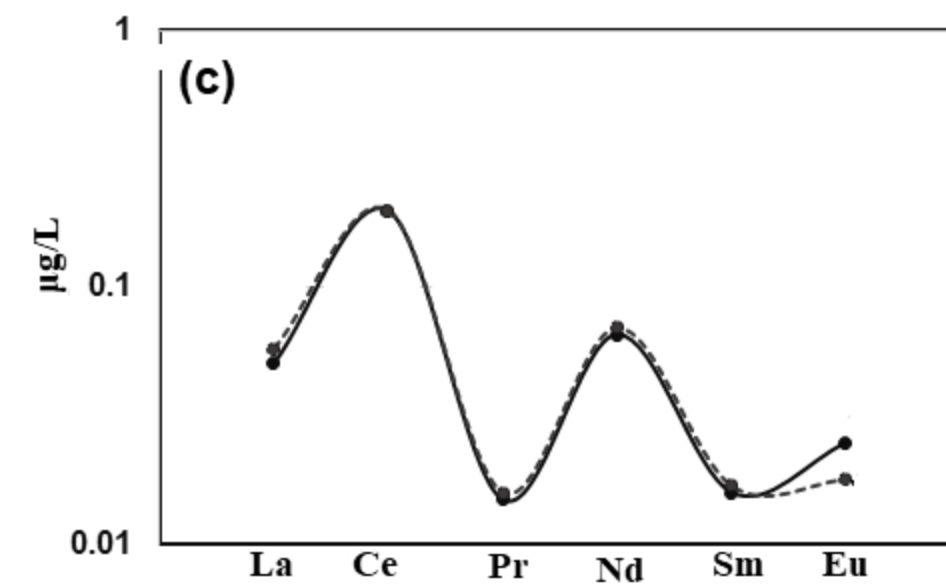
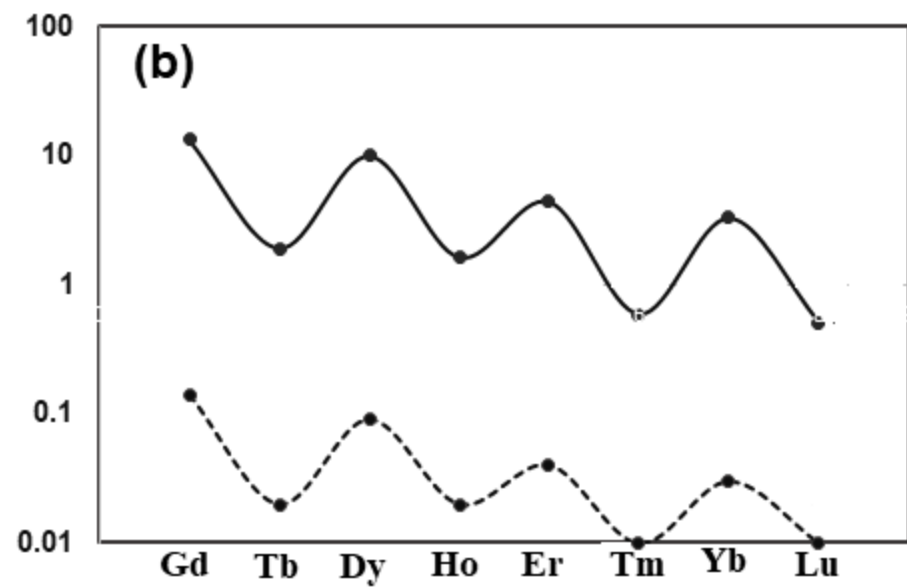
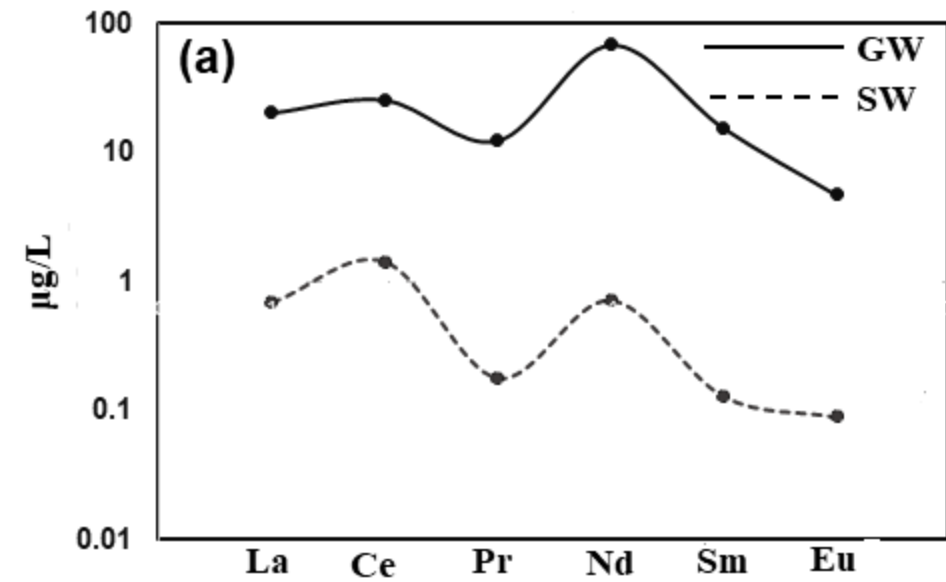


TBIW

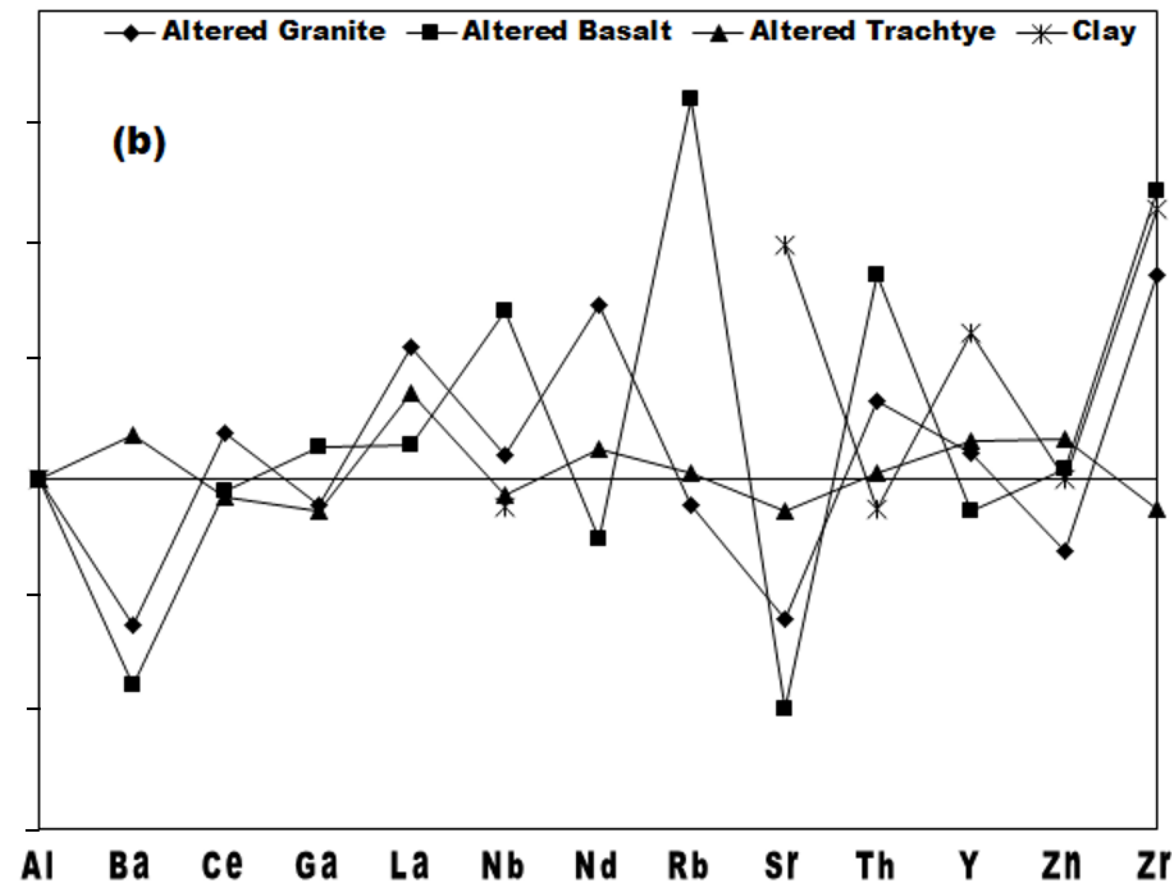
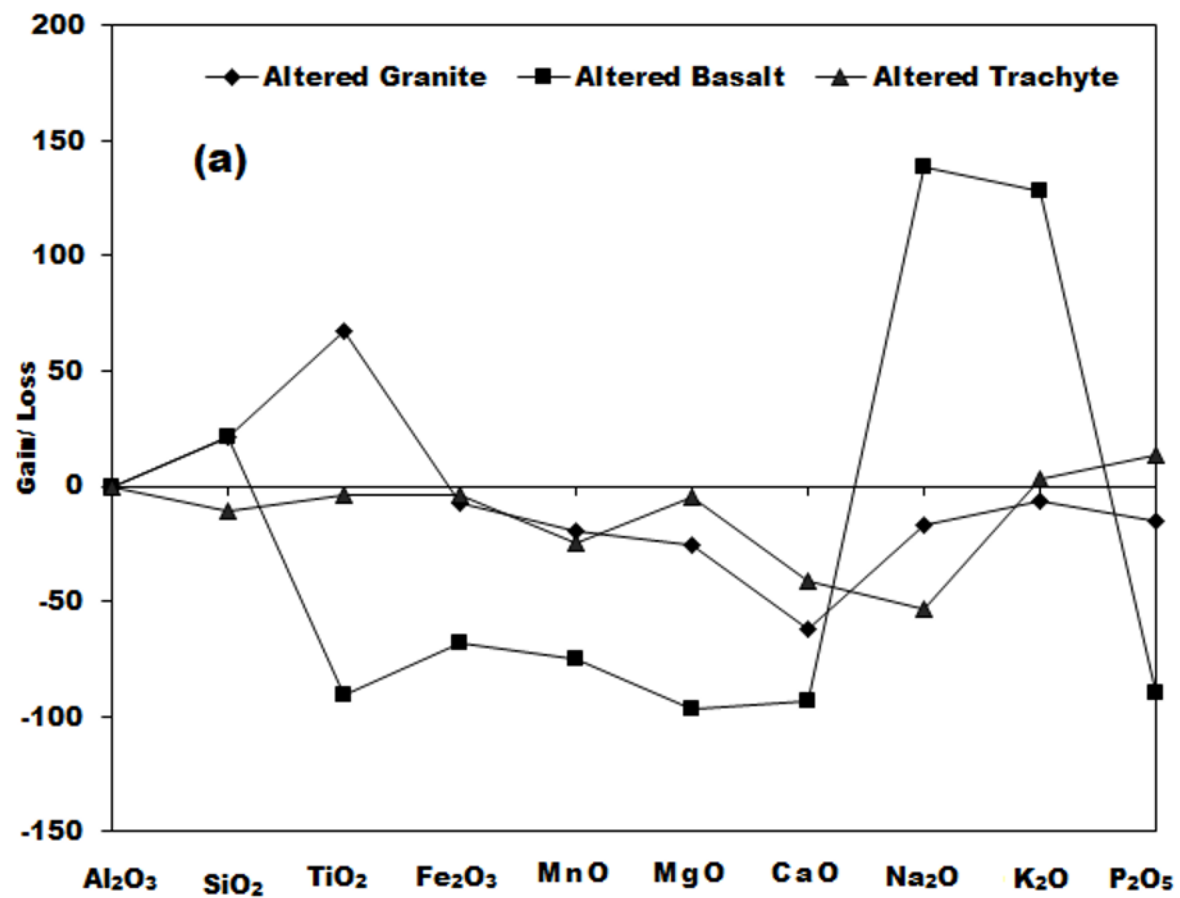


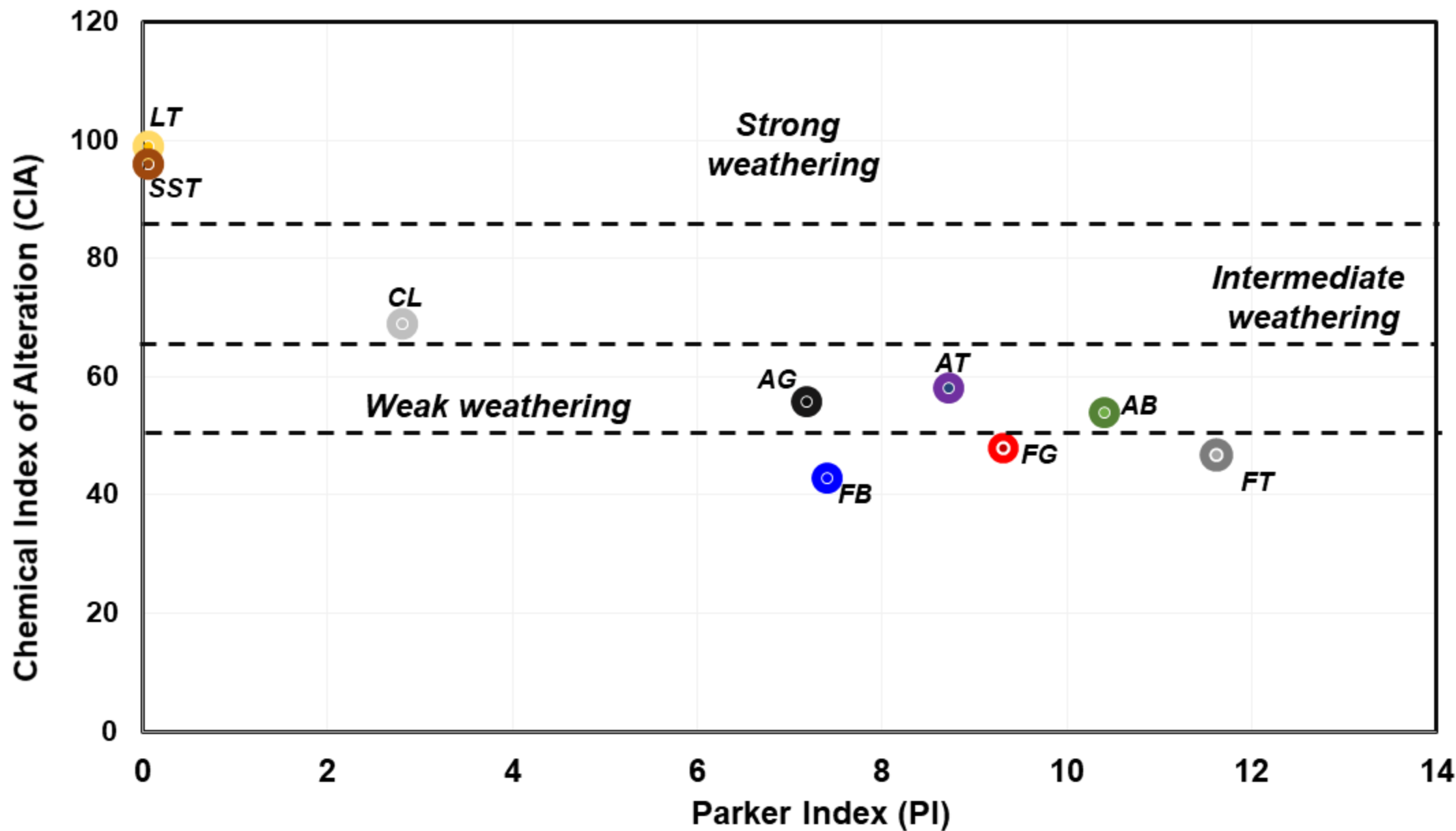


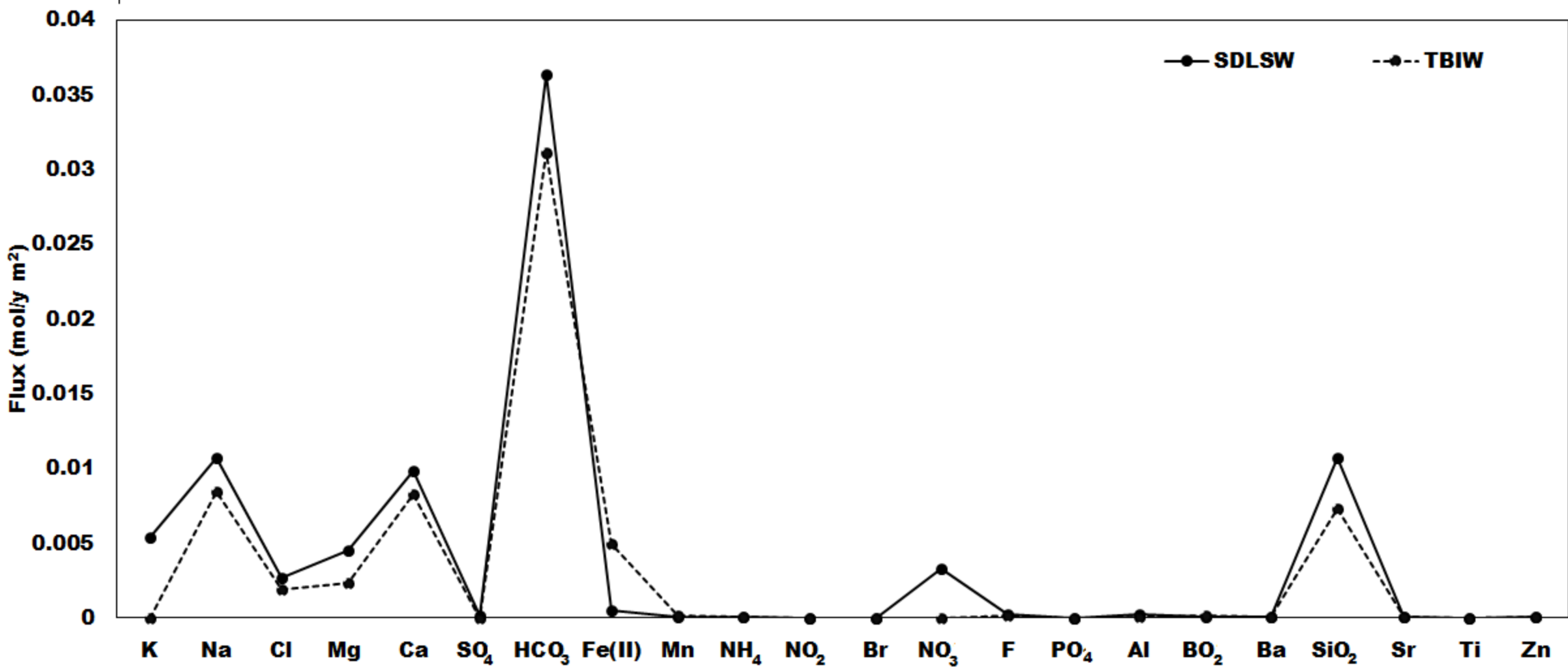




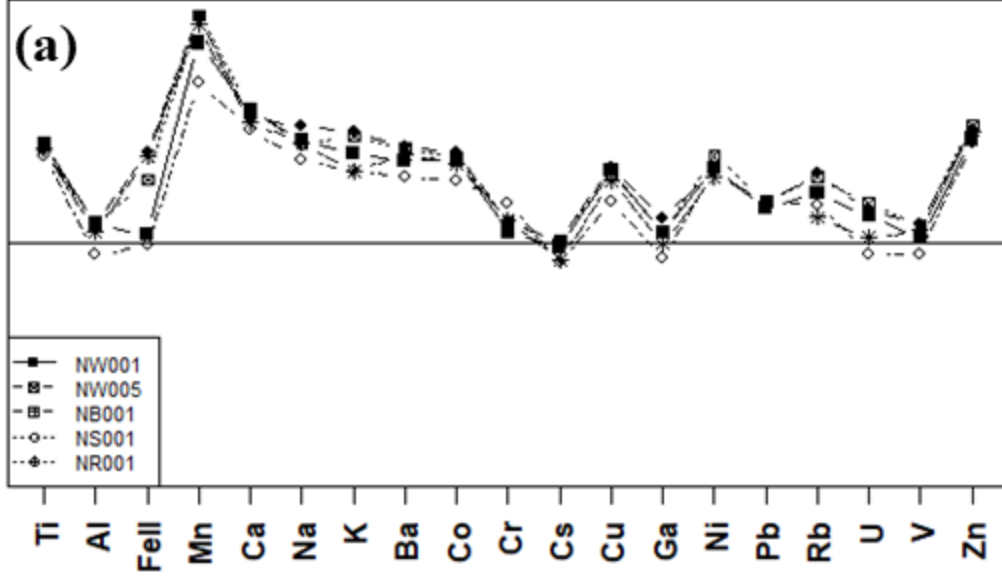




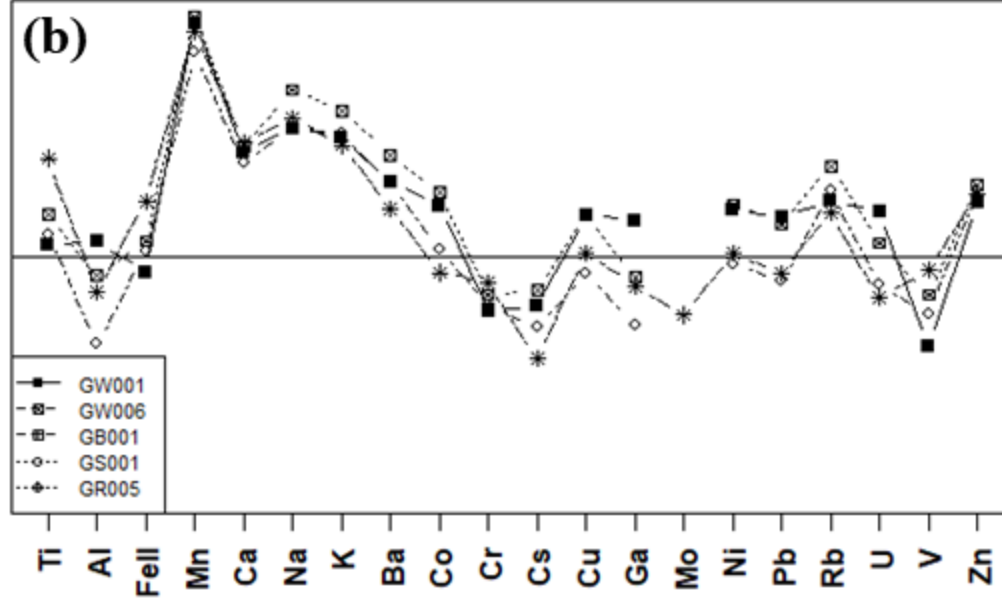




Relative mobility (RM)



Relative mobility (RM)



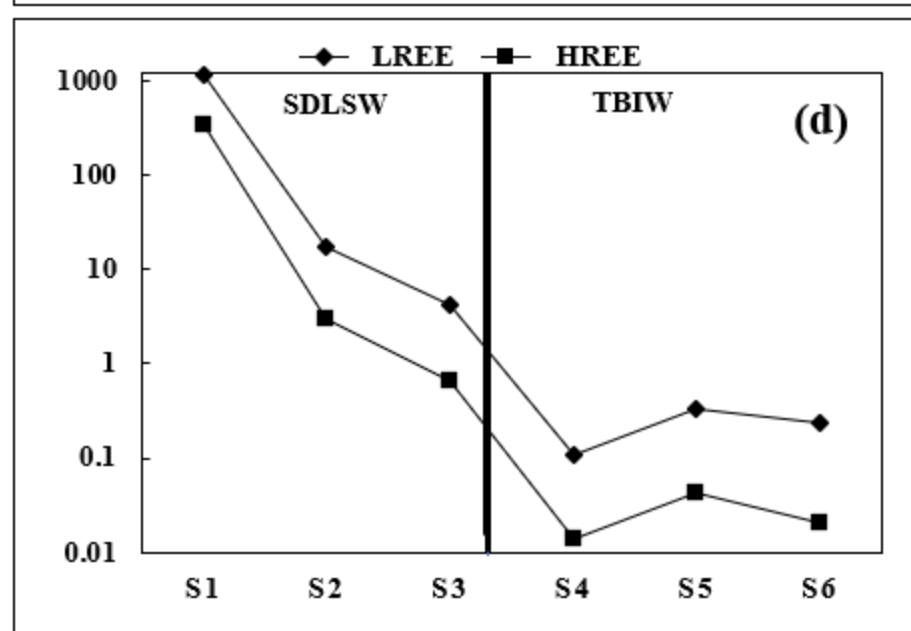
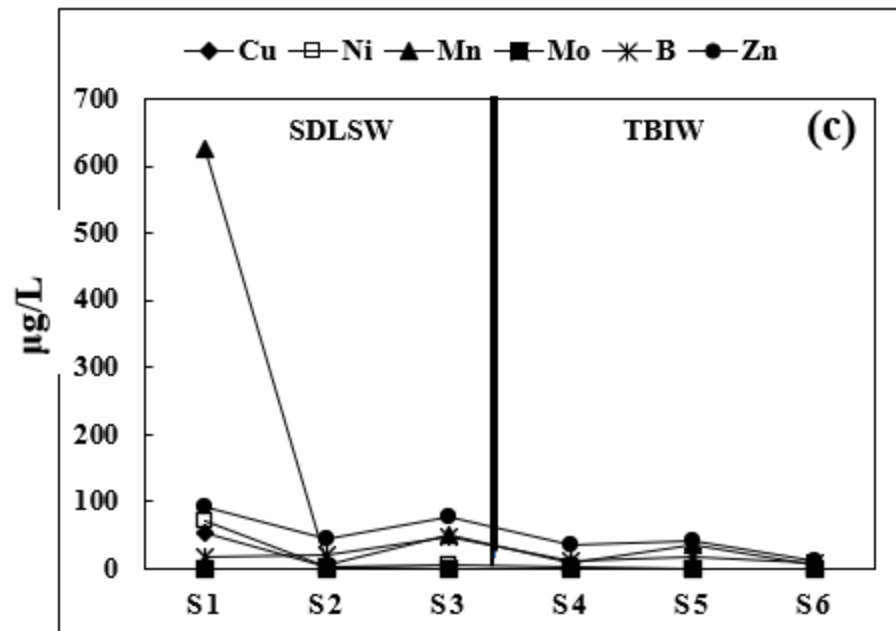
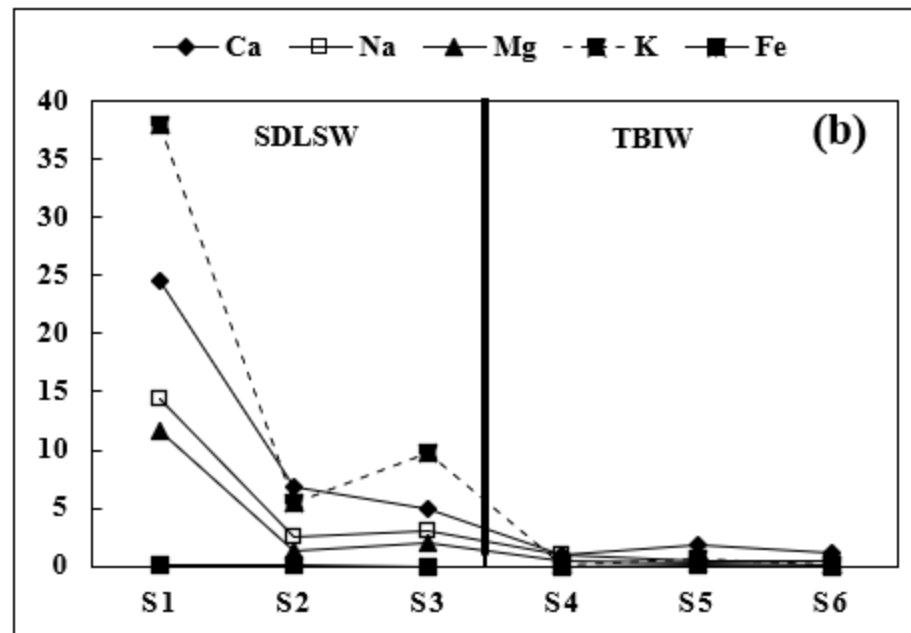
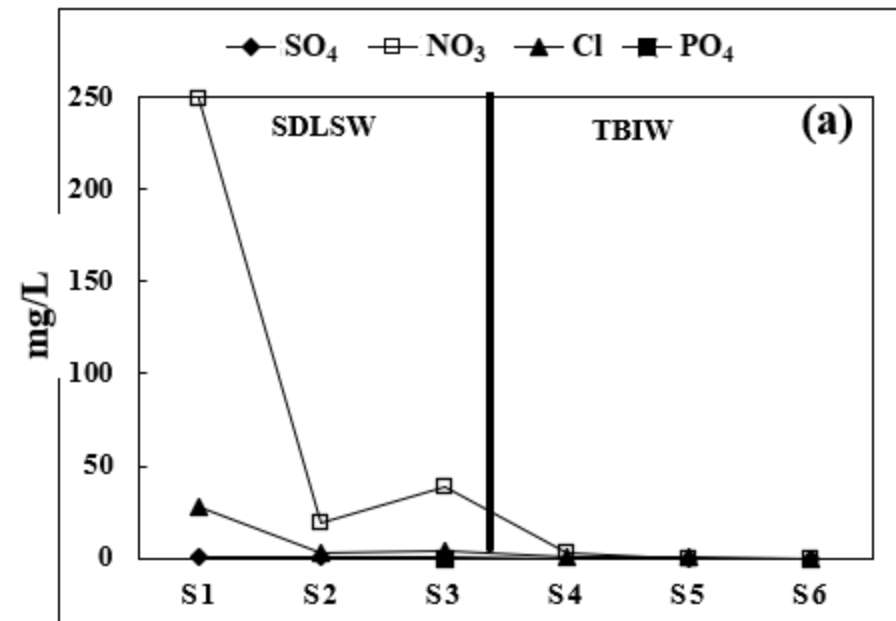


Table 1:

Parameter	Unit	Douka Longo watershed (SDLSW)					Bidou watershed (TBIW)				
		Min	Q25	Q50	Q75	Max	Min	Q25	Q50	Q75	Max
Temp	°C	26.5	28.9	29.9	30.6	34.0	19.5	22.3	23.7	25.0	26.1
pH	-	4.2	6.1	6.7	6.9	7.4	5.6	6.0	6.3	6.8	7.7
EC	μS/cm	58	82	110	221	698	9	14	19	32	160
Ca	mg/L	1.34	5.81	8.67	14.3	24.6	0.40	0.92	1.33	3.18	10.8
Mg	mg/L	0.400	1.70	2.55	4.70	11.6	0.076	0.227	0.238	1.35	5.05
Na	mg/L	1.4	3.2	5.4	6.8	27	0.4	0.6	1.1	2.0	25
K	mg/L	2.9	5.5	8.2	15.3	75.3	<0.1	0.2	0.4	0.9	1.5
HCO <sub>3</sub>	mg/L	1.7	8.6	19.9	40.8	55.5	3.3	5.4	10.0	17.6	66.4
SO <sub>4</sub>	mg/L	0.011	0.251	0.382	0.684	7.01	<0.003	0.012	0.021	0.040	18.7
Cl	mg/L	0.803	2.03	3.71	12.1	34.2	0.006	0.066	0.118	0.226	16.9
SiO <sub>2</sub>	mg/L	8.7	11.7	12.8	14.1	16.2	2.0	3.0	4.4	6.1	15.9
NH <sub>4</sub>	mg/L	<0.01	0.01	0.03	0.05	0.34	<0.01	<0.01	<0.01	0.04	0.88
NO <sub>3</sub>	mg/L	0.506	4.53	21.4	59.7	266	<0.003	0.052	0.215	0.788	37.9
Fe(II)	mg/L	0.005	0.015	0.049	0.443	1.94	0.003	0.014	0.054	0.487	1.58
Br	mg/L	<0.003	0.010	0.011	0.021	0.040	<0.003	<0.003	<0.003	<0.003	0.067
F	mg/L	0.018	0.032	0.085	0.100	0.941	0.005	0.012	0.021	0.043	0.148
δ <sup>18</sup> O	‰	-5.31	-4.77	-4.60	-4.42	-2.79	-4.51	-3.51	-3.39	-3.23	-0.86
δ <sup>2</sup> H	‰	-30.7	-27.3	-26.7	-24.4	-21.3	-24.5	-16.4	-15.7	-14.8	-11.5
DE	‰	1.0	9.3	10	11	12	-4.7	11	12	12	13
pCO <sub>2</sub>	atm	0.001	0.002	0.005	0.007	0.009	0.002	0.003	0.005	0.008	0.014

Min=Minimum, Max=Maximum, DE=Deuterium excess, Temp = Temperature, EC = Electrical Conductivity

Table 2:

Parameter	Unit	Douka Longo watershed (SDLSW)					Bidou watershed (TBIW)				
		Min	Q25	Q50	Q75	Max	Min	Q25	Q50	Q75	Max
Ag	µg/L	<0.003	<0.003	<0.003	<0.003	0.033	All concentrations <0.003				
As	µg/L	0.022	0.043	0.117	0.187	17.1	<0.010	0.010	0.025	0.045	0.108
B	µg/L	6.35	10.9	17.8	21.5	64.4	2.39	8.02	11.0	14.2	20.0
Ba	µg/L	165	246	315	876	3921	18.9	43.5	54.2	65.2	141
Be	µg/L	0.031	0.079	0.288	0.609	22.9	<0.007	<0.007	0.036	0.076	0.298
Bi	µg/L	<0.002	<0.002	<0.002	<0.002	0.003	All concentrations <0.002				
Cd	µg/L	<0.002	0.005	0.009	0.013	0.214	<0.002	0.002	0.005	0.006	0.032
Co	µg/L	0.123	0.463	1.42	5.12	108	0.062	0.363	0.651	1.09	6.22
Cr	µg/L	0.058	0.180	0.232	0.443	1.65	0.027	0.083	0.130	0.224	2.00
Cs	µg/L	0.013	0.034	0.129	0.201	2.41	<0.003	0.006	0.009	0.014	0.129
Cu	µg/L	0.276	0.711	1.06	1.69	54.5	0.071	0.259	0.366	0.456	1.01
Ga	µg/L	0.028	0.050	0.121	0.236	40.3	<0.002	0.009	0.016	0.024	0.044
Hf	µg/L	<0.002	<0.002	0.005	0.020	0.159	<0.002	<0.002	<0.002	<0.002	0.004
In	µg/L	0.026	0.026	0.026	0.027	0.028	0.026	0.026	0.026	0.026	0.027
Li	µg/L	0.452	0.921	1.90	3.87	22.1	0.108	0.210	0.302	0.531	1.12
Mn	µg/L	6.63	30.6	46.1	66.1	1755	2.03	13.7	26.0	41.0	407
Mo	µg/L	<0.020	<0.020	<0.020	0.040	0.260	<0.020	<0.020	<0.020	<0.020	0.068
Nd	µg/L	0.180	0.515	0.807	1.66	658	0.005	0.030	0.051	0.090	0.229
Ni	µg/L	0.652	1.19	2.95	6.18	72.7	<0.200	0.317	0.541	1.07	5.89
Pb	µg/L	0.073	0.042	0.475	0.758	56.3	<0.020	0.030	0.045	0.054	0.260
Rb	µg/L	7.20	13.0	22.1	40.2	83.5	0.112	0.680	1.46	2.44	4.08
Sb	µg/L	<0.005	0.007	0.011	0.016	0.158	<0.005	<0.005	<0.005	0.008	0.018
Sc	µg/L	0.138	0.192	0.265	0.317	0.609	<0.020	0.061	0.093	0.130	0.206
Sn	µg/L	<0.020	<0.020	<0.020	0.022	0.222	All concentrations <0.020				
Sr	µg/L	0.138	0.192	0.265	0.317	0.609	4.68	12.0	14.7	45.7	115
Ta	µg/L	<0.001	<0.001	0.002	0.007	0.031	All concentrations <0.001				
Te	µg/L	<0.010	<0.010	<0.010	0.030	0.061	<0.010	<0.010	0.011	0.021	0.042
Th	µg/L	<0.004	<0.004	0.020	0.069	0.213	<0.004	<0.004	<0.004	<0.004	0.005
Ti	µg/L	0.092	0.252	1.93	7.50	53.8	0.064	0.100	0.206	0.306	2.57
Tl	µg/L	0.022	0.030	0.114	0.207	1.23	<0.003	0.004	0.005	0.008	0.053
U	µg/L	0.008	0.045	0.094	0.295	66.7	0.001	0.003	0.005	0.008	0.018
V	µg/L	0.070	0.215	0.495	1.11	1.39	<0.007	0.036	0.062	0.155	1.42
W	µg/L	<0.050	<0.050	<0.050	<0.050	0.139	All concentrations <0.050				
Y	µg/L	0.115	0.366	0.557	1.17	485	0.014	0.034	0.052	0.116	0.302
Zn	µg/L	8.44	25.5	38.2	73.8	139	2.48	27.1	33.7	37.1	70.5
Zr	µg/L	<0.005	0.024	0.077	0.199	1.38	<0.005	0.006	0.009	0.017	0.081

Min = Minimum, Max = Maximum

Table 3:

Parameter	Unit	Douka Longo watershed (SDLSW)					Bidou watershed (TBIW)				
		Min	Q25	Q50	Q75	Max	Min	Q25	Q50	Q75	Max
La	µg/L	0.185	0.548	0.818	1.19	193	0.009	0.025	0.042	0.069	0.206
Ce	µg/L	0.110	0.575	0.998	1.83	273	0.025	0.054	0.110	0.197	2.05
Pr	µg/L	0.042	0.130	0.207	0.368	119	0.002	0.009	0.012	0.019	0.053
Nd	µg/L	0.180	0.515	0.807	1.66	658	0.005	0.030	0.051	0.090	0.229
Sm	µg/L	0.036	0.082	0.181	0.371	139	0.002	0.009	0.014	0.020	0.049
Eu	µg/L	0.062	0.124	0.204	0.341	41.6	0.008	0.016	0.021	0.026	0.055
Gd	µg/L	0.041	0.086	0.166	0.381	121	0.004	0.008	0.014	0.020	0.044
Tb	µg/L	0.004	0.011	0.020	0.049	17.9	<0.001	0.001	0.002	0.003	0.007
Dy	µg/L	0.024	0.068	0.106	0.257	95.4	<0.001	0.005	0.009	0.017	0.038
Ho	µg/L	0.003	0.012	0.019	0.042	15.7	<0.001	0.001	0.002	0.003	0.006
Er	µg/L	0.010	0.030	0.051	0.110	43.2	<0.001	0.003	0.006	0.008	0.026
Tm	µg/L	0.001	0.004	0.008	0.015	5.76	<0.001	<0.001	<0.001	0.002	0.003
Yb	µg/L	0.007	0.024	0.045	0.098	32.3	<0.001	0.003	0.005	0.009	0.025
Lu	µg/L	<0.001	0.004	0.007	0.014	4.88	<0.001	<0.001	<0.001	0.002	0.005
ΣREE	µg/L	0.916	1.97	4.09	6.08	1716	0.085	0.184	0.261	0.518	2.37
ΣLREE	µg/L	0.634	1.44	3.27	5.17	1243	0.041	0.133	0.210	0.420	2.22
ΣHREE	µg/L	0.050	0.158	0.275	0.585	215	0.002	0.014	0.025	0.036	0.097
ΣMREE	µg/L	0.156	0.400	0.541	0.905	298	0.017	0.037	0.051	0.059	0.130
ΣLREE/ΣHREE	µg/L	4.50	8.73	10.6	13.1	17.5	2.39	5.96	10.2	13.9	71.5
Eu/Eu*	-	1.37	2.53	3.94	9.25	42.7	2.32	4.22	7.05	10.8	22.1
Ce/Ce*	-	0.084	0.353	0.565	0.835	1.14	0.331	0.842	1.28	1.73	11.2
La/Yb	-	4.65	13.4	17.3	21.9	31.1	0.929	4.69	7.89	13.2	>24.0
La/Sm	-	1.11	3.52	4.35	5.18	8.18	1.18	2.32	3.00	4.26	12.0
Gd/Dy	-	0.981	1.38	1.46	1.54	2.17	0.786	1.17	1.53	2.26	>7.00



Table 4:

Parameters	Units	Fresh Granite	Altered Granite	Fresh Basalt	Altered Basalt	Fresh Trachyte	Altered Trachyte	Laterite	Sandstone	Clay	
SiO2	%	70.55	74.86	45.32	62.31	56.54	55.72	8.81	95.22	83.07	
TiO2	%	0.170	0.248	3.244	0.340	0.605	0.647	1.436	0.103	0.624	
Al2O3	%	15.72	13.71	16.11	18.21	19.02	21.10	9.11	3.09	7.61	
Fe2O3	%	1.20	0.97	12.04	4.30	3.57	3.80	64.88	0.09	1.29	
MnO	%	0.027	0.019	0.241	0.068	0.245	0.204	0.098	<0.001	0.036	
MgO	%	0.17	0.11	4.92	0.18	0.52	0.55	0.03	0.01	0.10	
CaO	%	0.788	0.264	8.529	0.642	2.395	1.571	0.031	0.049	0.116	
Na2O	%	3.78	2.73	2.27	6.12	7.35	3.83	<0.01	<0.01	0.12	
K2O	%	6.555	5.348	2.065	5.327	4.766	5.446	0.037	0.032	3.093	
P2O5	%	0.035	0.026	1.289	0.146	0.165	0.208	1.648	0.013	0.029	
(SO3)	%	0.02	<0.01	<0.01	<0.01	0.08	<0.01	<0.01	<0.01	<0.01	
(Cl)	%	0.003	0.005	0.014	0.002	0.017	0.005	0.002	0.004	<0.002	
(F)	%	<0.05	<0.05	<0.05	<0.05	<0.05	<0.05	<0.05	<0.05	<0.05	
LOI	%	0.73	1.55	3.37	2.06	4.10	6.18	13.63	1.35	3.62	
Sum	%	99.73	99.76	99.44	99.66	99.29	99.22	99.66	99.87	99.63	
(As)	mg/kg	<3	<3	<4	<3	7	4	<5	<3	<3	
Ba	mg/kg		485	159	1131	150	1464	2026	198	<62	843
Bi	mg/kg	<6	<6	<7	<6	<6	<6	<10	<5	<6	
Ce	mg/kg		126	131	166	176	213	229	<57	<54	62
Co	mg/kg	<8		8	32	<8	<8		48	<7	<8
Cr	mg/kg	<12	<11		51	<12	<12		543	<11	27
Cs	mg/kg	<57	<54	<60	<57	<57	<57	<54	<54	<54	
Cu	mg/kg		8	<6	19	<6	16	10	53	<6	8
Ga	mg/kg		26	20	22	28	25	25	<9	<5	10
Hf	mg/kg	<18	<18	<22	<19		20	26	<34	<17	<18
La	mg/kg		64	87	88	113	125	199	<49	<47	<47
Mo	mg/kg	<8	<8	<8	<8	<8	<8	<8	<8	<7	
Nb	mg/kg		24	23	83	160	141	152	33	6	13
Nd	mg/kg		58	88	78	65	68	89	<52	<39	<39
Ni	mg/kg		6	<6	41	<6	<6		56	<6	9
Pb	mg/kg		48	36	<8	8	13	<7	<11	<7	20
Rb	mg/kg		339	261	38	112	127	151	<7	<4	86

Sb	mg/kg	<21	<19	<23	<21	<21	<21	<33	<19	<20
Sc	mg/kg	<26	<26	<28	<26	<26	<26	<26	<26	<26
Sm	mg/kg	<25	<24	<26	<24	<25	<24	39	<23	<24
Sn	mg/kg	<18	<17	<21	<18	<18	<18	<31	<17	<17
Sr	mg/kg	118	41	1573	19	1128	1135	80	24	118
Ta	mg/kg	<12	<11	<14	<12	<12	<12	<24	<11	<11
Th	mg/kg	31	36	10	21	21	25	11	7	15
U	mg/kg	<6	6	<7	<6	<6	<6	<9	<6	<6
V	mg/kg	<17	<17	154	<17	<17	19	398	<16	34
W	mg/kg	<11	<11	<13	<11	<11	<11	<22	<10	<11
Y	mg/kg	26	25	36	35	37	50	34	7	28
Zn	mg/kg	45	27	137	160	175	238	108	<5	14
Zr	mg/kg	115	187	324	813	1241	1259	142	152	805

Table 5.

Rock types	State of alteration	Silica content (Wt %)	Average density (kg/m <sup>3</sup> )	Chemical composition S (kg/m <sup>3</sup> )	So-Ss	QSiO <sub>2</sub> (mol/y m <sup>2</sup> )	WRch (mm/yr)
Granite	Fresh	70.55	2600	1834.3	786.26	0.007324	<b>0.0006</b>
	Altered	74.86	1400	1048.04			
Basalt	Fresh	45.32	2600	1178.32	305.98		<b>0.0014</b>
	Altered	62.31	1400	872.34			
Trachyte	Fresh	56.54	2600	1470.04	689.96		<b>0.0006</b>
	Altered	55.72	1400	780.08			
Sandstone	-	95.22	2600	2475.72	1312.74	0.010701	<b>0.0005</b>
Clay	-	83.07	1400	1162.98			

**Table 6a.**

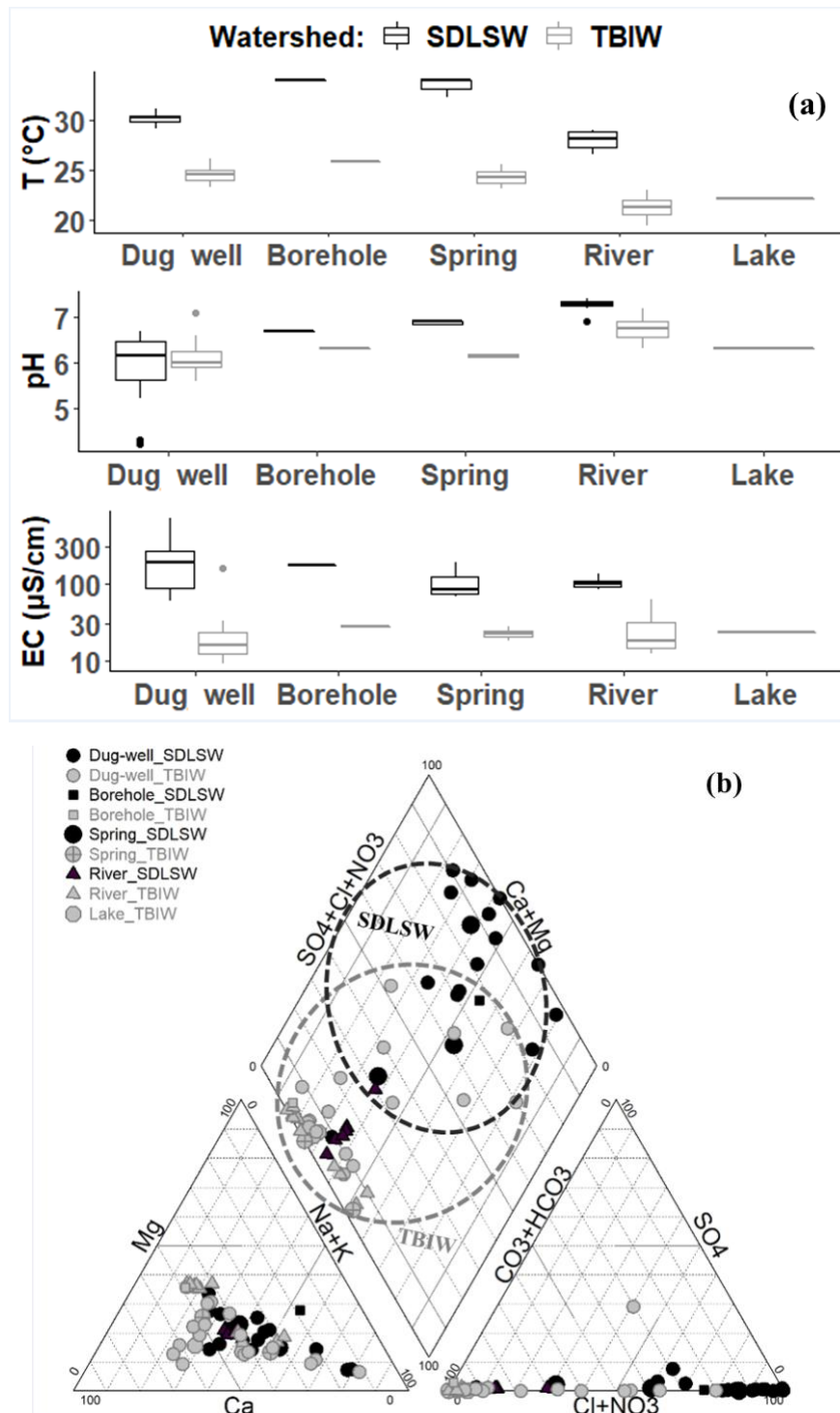
	Units	Na <sup>+</sup>	K <sup>+</sup>	Mg <sup>2+</sup>	Ca <sup>2+</sup>	SiO <sub>2</sub>	HCO <sub>3</sub> <sup>-</sup>	SO <sub>4</sub> <sup>2-</sup>	Cl <sup>-</sup>	mg	Wt. %
Analysis	mg/L	7.38	14.35	3.67	10.97	13.06	27.87	0.93	9.28		
	μmol/L	321	368	153	274	218	457	10	262		
Rainfall	μmol/L	64	41	26	46	5	27	8	22		
Net (analysis – rainfall)	μmol/L	257	327	127	228	212	430	2	240		
Ion balance	μeq/L	1294					-674				
Adjusted	μmol/L	257	327	127	228	212	1050	2	240		
Albite	μmol/L	0	327	127	228	0	793	2	240	67	25
K-feldspar	μmol/L	0	0	127	228	0	466	2	240	91	34
Biotite	μmol/L	0	0	0	228	0	148	2	240	28	11
Anorthite	μmol/L	0	0	0	0	0	0	2	240	63	24
Gypsum	μmol/L	0	0	0	0	0	0	0	240	0.344	0.13
Halite	μmol/L	0	0	0	0	0	0	0	0	14.04	5.30
										<b>265</b>	<b>100</b>

Assuming all the sulphate and chloride come from gypsum and halite respectively

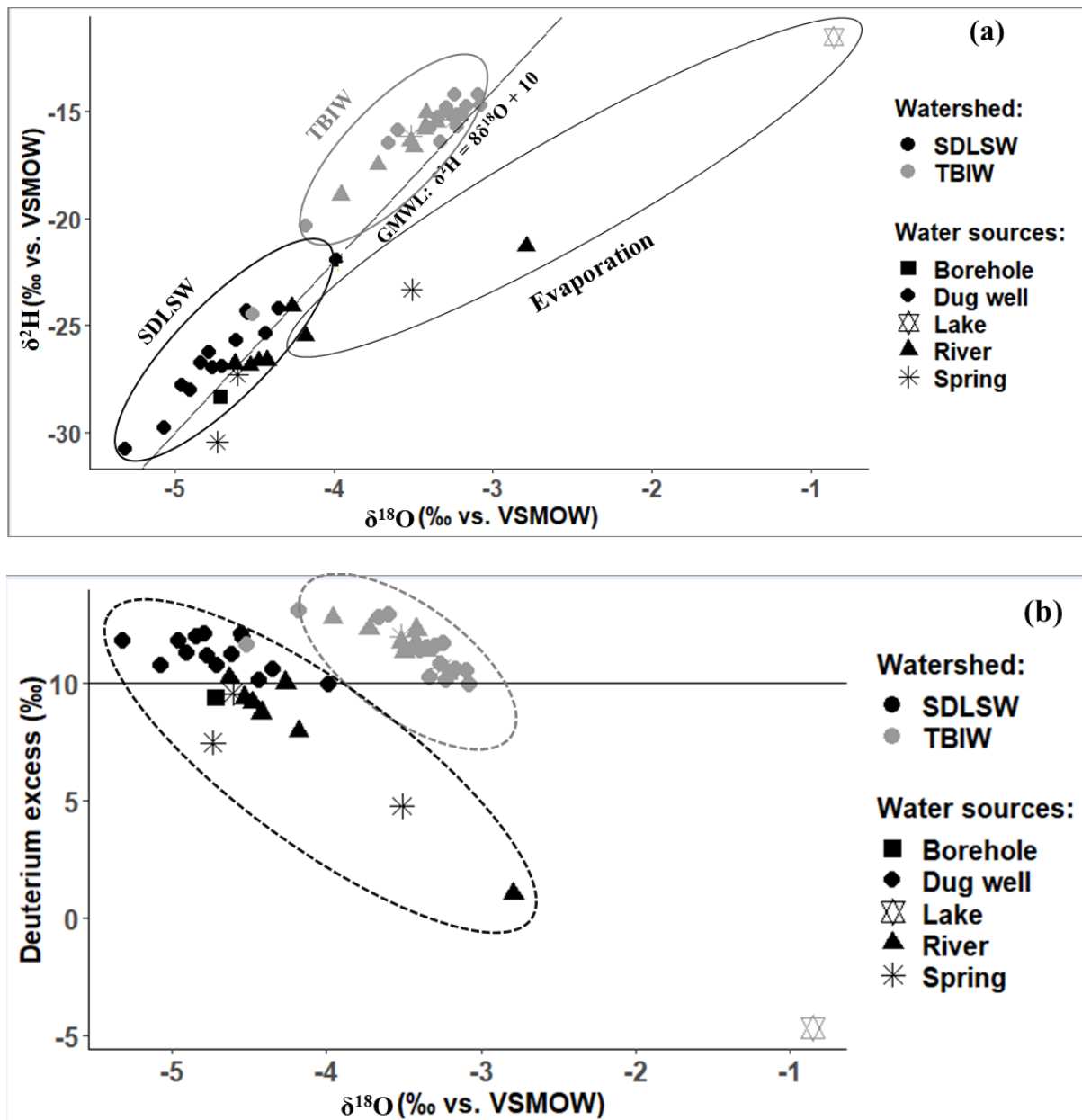
**Table 6b.**

	Units	Na <sup>+</sup>	K <sup>+</sup>	Mg <sup>2+</sup>	Ca <sup>2+</sup>	SiO <sub>2</sub>	HCO <sub>3</sub> <sup>-</sup>	SO <sub>4</sub> <sup>2-</sup>	Cl <sup>-</sup>	mg	Wt. %
Analysis	mg/L	2.50	1.20	1.18	2.98	6.31	15.06	0.54	1.40		
	μmol/L	109	31	49	74	105	247	6	39		
Rainfall	μmol/L	43	21	17	31	3	18	4	15		
Net (analysis – rainfall)	μmol/L	66	10	32	43	102	229	2	24		
Ion balance	μeq/L	226+					257-				
Adjusted	μmol/L	66	10	32	43	102	198	2	24		
Albite	μmol/L	0	10	32	43	0	132	2	24	17	42
K-feldspar	μmol/L	0	0	32	43	0	122	2	24	3	7
Biotite	μmol/L	0	0	32	0	0	36	2	24	12	29
Anorthite	μmol/L	0	0	0	0	0	0	2	24	7	18
Gypsum	μmol/L	0	0	0	0	0	0	0	24	0.3	1
Halite	μmol/L	0	0	0	0	0	0	0	0	1.4	3
										<b>50</b>	<b>100</b>

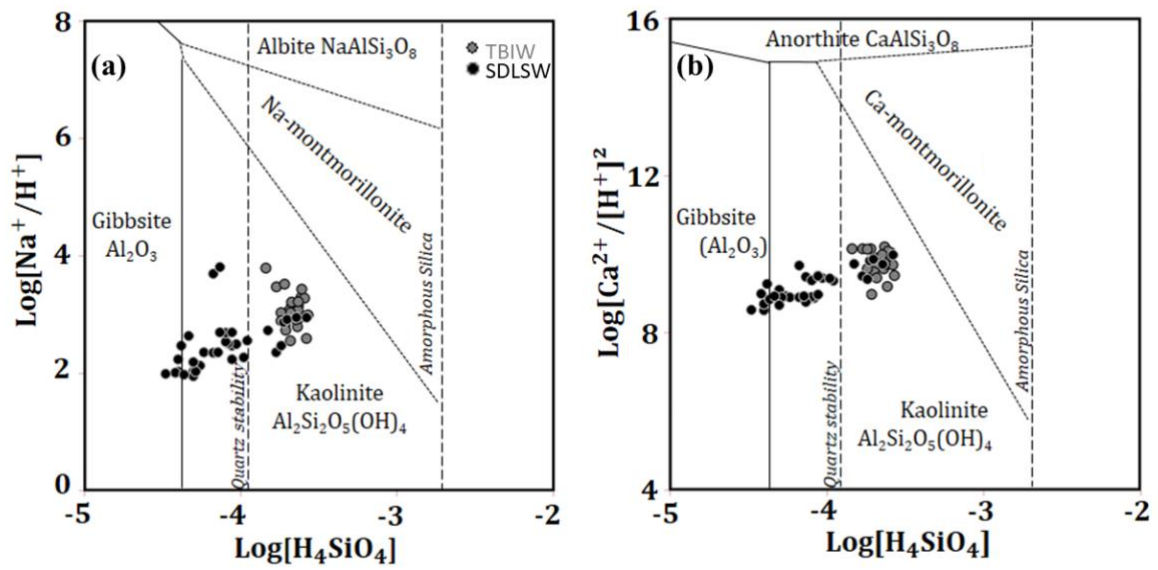
Assuming all the sulphate and chloride come from gypsum and halite respectively



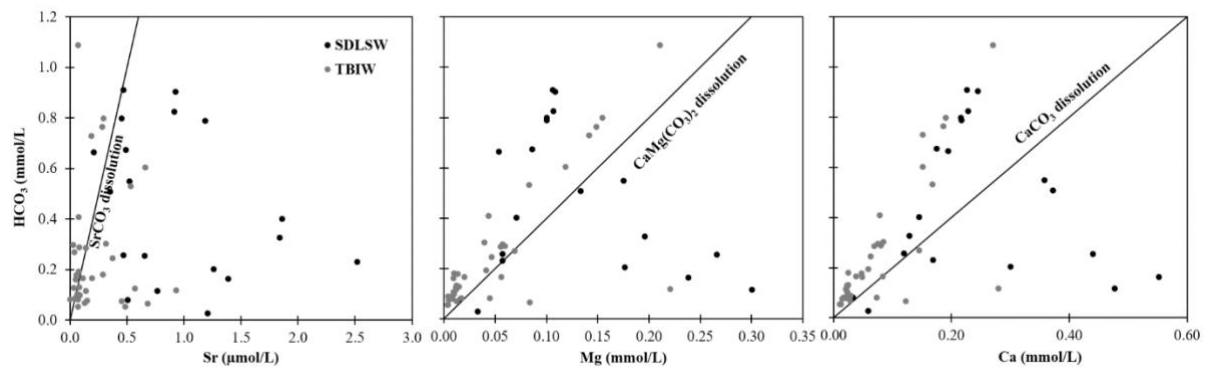
SM1a-b. Physico-chemical results: (a) Variations of water temperature , pH , and EC according to sampling point type. The bottom and top edges of the box indicate the 25<sup>th</sup> and 75<sup>th</sup> percentiles, respectively. The maximum whisker length is 1.5 times the difference between the 25<sup>th</sup> and 75<sup>th</sup> percentiles. Points not included within the whiskers are plotted individually as outliers (symbol ●). (b) Piper diagram with samples from both watersheds. The circles indicate where most of groundwater samples are plotted for each watershed.



SM2a-b. (a) Water stable isotopes  $\delta^{18}\text{O}$  and  $\delta\text{D}$  in both watersheds. Most samples plot along the Global Meteoric Water Line (GMWL) of Craig (1961), indicating groundwater recharge with little or no evaporation. A few surface water samples plot to the right of the GMWL, indicating evaporation. (b) Deuterium excess: more than 80 % of water (mostly from hand dug wells) in the SDLSW show d-excess greater than 10 ‰ and all water samples from the TBIW show d-excess greater than 10 ‰, indicating recharge under high humidity and temperature conditions in both watersheds.



SM3. Stability diagrams at 25° C: (a) albite system, and (b) anorthite system. In both systems, the water samples are in equilibrium with gibbsite and kaolinite.



SM4. Identification of minerals undergoing dissolution: bivariate plots of (a) Mg vs.  $\text{HCO}_3^-$ , (dolomite  $\text{CaMg}(\text{CO}_3)_2$ ); (b) Sr vs  $\text{HCO}_3^-$  (strontianite  $\text{SrCO}_3$ ); and (c) Ca vs  $\text{HCO}_3^-$  (calcite  $\text{CaCO}_3$ ).